
LONG-TIME INTEGRATION OF PARAMETRIC EVOLUTION EQUATIONS WITH PHYSICS-INFORMED DEEPONETS

A PREPRINT

Sifan Wang

Graduate Group in Applied Mathematics
and Computational Science
University of Pennsylvania
Philadelphia, PA 19104
sifanw@sas.upenn.edu

Paris Perdikaris

Department of Mechanical Engineering
and Applied Mechanics
University of Pennsylvania
Philadelphia, PA 19104
pgp@seas.upenn.edu

June 11, 2021

ABSTRACT

Ordinary and partial differential equations (ODEs/PDEs) play a paramount role in analyzing and simulating complex dynamic processes across all corners of science and engineering. In recent years machine learning tools are aspiring to introduce new effective ways of simulating PDEs, however existing approaches are not able to reliably return stable and accurate predictions across long temporal horizons. We aim to address this challenge by introducing an effective framework for learning infinite-dimensional operators that map random initial conditions to associated PDE solutions within a short time interval. Such latent operators can be parametrized by deep neural networks that are trained in an entirely self-supervised manner without requiring any paired input-output observations. Global long-time predictions across a range of initial conditions can be then obtained by iteratively evaluating the trained model using each prediction as the initial condition for the next evaluation step. This introduces a new approach to temporal domain decomposition that is shown to be effective in performing accurate long-time simulations for a wide range of parametric ODE and PDE systems, from wave propagation, to reaction-diffusion dynamics and stiff chemical kinetics, all at a fraction of the computational cost needed by classical numerical solvers.

Keywords Deep learning · Computational science · Differential equations · Dynamical systems

1 Introduction

Evolution equations, typically expressed as systems of time-dependent ordinary or partial differential equations (ODEs/PDEs), play a prominent role in the analysis, modeling and simulation of complex dynamical systems across diverse scientific domains, from fluid mechanics, to electromagnetics, quantum mechanics, and elasticity [1]. Classical approaches to simulating such equations often assume a discrete, finite-dimensional representation of the unknown solution (typically parametrized by a linear combination of fixed features such as polynomials, trigonometric functions, etc.), the weights of which are inferred by solving large linear or nonlinear systems, depending on the nature of the underlying equation and the scheme used to discretize it [2]. For time-dependent problems these weights vary with time, and can be iteratively updated via appropriate time-integration schemes that discretize the temporal prediction horizon into a small number of steps, the size of which is dictated by the governing time-scales of the problem and the stability properties of the temporal discretization employed [3]. This general workflow has been thoroughly studied over the last several decades, leading to robust and provably accurate techniques such as the finite-element method [4], Runge-Kutta schemes [3], and Krylov subspace methods [5] that serve as the main workhorses of modern computational science and engineering. But as the complexity of the underlying evolution equations increases, so does the cost of simulating them; a cost that quickly becomes unbearable when multiple scenarios need to be queried (e.g., corresponding to different initial and boundary conditions (IBCs), random inputs, forcing terms, etc.), and/or when multi-scale interactions dictate the underlying dynamics.

As the machine learning (ML) revolution is persistently reaching all corners of science, a new wave of techniques are being proposed for accelerating the simulation of ODEs and PDEs [6]. Instead of representing the target solution using a set of fixed features that are determined a-priori, neural networks [7, 8] and kernel machines [9, 10] offer the possibility of learning effective representations that are adapted to the underlying evolution law. A representative example is the framework of physics-informed neural networks (PINNs) [11] that opts to represent the entire spatio-temporal solution of a PDE system using a single deep neural network that is trained to jointly fit observed data (e.g., IBCs), as well as ensure that the predicted solution satisfies the underlying system of PDEs by minimizing its residual. An attractive property of this approach is that it no longer requires a spatial or temporal discretization of the PDE, nor it requires any external training data (other than knowledge of appropriate IBCs). Moreover, the entire global solution can be rapidly obtained once the network has been trained [11]. However, this remarkable flexibility often comes at the price of reduced accuracy, as well as a multitude of caveats that hinder the training and convergence of such models [12, 13, 14]. Nevertheless, PINNs [15], their variants [16, 17, 18], and other ML-based approaches [19, 20, 21] are currently enjoying increased popularity across diverse applications including fluid mechanics [22, 23], heat transfer [24, 25], bio-engineering [26, 27], materials [28, 29, 30], and finance [31, 32]. However, a major challenge still remains unsolved and has been largely overlooked in the existing literature: ML-based approaches often fail to accurately simulate evolution equations over a long-time prediction horizon.

In this work we attempt to address this fundamental challenge by leveraging the recently developed framework of physics-informed deep operator networks (DeepOnets) [33] to parametrize and learn the solution operator that maps random initial conditions to their associated ODE/PDE solutions within a short time interval. The proposed deep learning model can be trained in an entirely self-supervised manner (i.e. without the need for any paired input-output data), only assuming knowledge of the ODE/PDE model form and its associated IBCs. Once the model has been trained on a collection of initial conditions, it can be used to construct the global ODE/PDE solution across a long-time prediction horizons via a simple iterative procedure in which the model prediction over a short time-step is used as an initial condition for the next evaluation. We demonstrate that this approach can effectively enable the long-time integration of the evolution equations subject to a range of initial conditions with good generalization accuracy, all at a fraction of the computational cost needed by classical numerical solvers. Taken together, the computational infrastructure developed in this work can have a broad technical impact in significantly reducing computational costs and accelerating scientific modeling of complex non-linear, non-equilibrium processes across diverse applications.

The remaining of this paper is structured as follows. In section 2, we provide an overview of the PINNs framework put forth by Raissi *et al.* [11] and demonstrate its fundamental limitations in approximating ODE/PDE solutions over long-time horizons. Section 3 provides a detailed discussion of our main technical contributions, starting with a recap on physics-informed DeepOnets [33] in section 3.1, followed by the proposed formulation for tackling long-time integration problems in section 3.2. Further, in section 4 we present a series of comprehensive numerical studies to assess the performance of the proposed long-time integration framework across a range of parametric ODE/PDE systems involving wave propagation, reaction-diffusion dynamics, and stiff chemical kinetics. Finally, section 5 concludes with a discussion of our main findings, potential pitfalls, and shortcomings, as well as future research directions emanating from this study. All code and data accompanying this manuscript will be made available at <https://github.com/PredictiveIntelligenceLab/Long-time-Integration-PI-DeepONets>.

2 Physics-informed neural networks

In this section, we give a brief review of physics-informed neural networks (PINNs) [15] for solving time-dependent ODEs and PDEs. Generally, we consider initial-boundary value problems taking the form

$$\mathbf{s}_t + \mathcal{N}_{\mathbf{x}}[\mathbf{s}] = \mathbf{0}, \quad \mathbf{x} \in \Omega, t \in [0, T] \quad (2.1)$$

$$\mathbf{s}(\mathbf{x}, t) = \mathbf{g}(\mathbf{x}, t), \quad \mathbf{x} \in \partial\Omega, t \in [0, T] \quad (2.2)$$

$$\mathbf{s}(\mathbf{x}, 0) = \mathbf{u}(\mathbf{x}), \quad \mathbf{x} \in \Omega, \quad (2.3)$$

where \mathbf{x} and t represent spatial and temporal coordinates, respectively, $\mathcal{N}_{\mathbf{x}}$ denotes a differential operator with respect to \mathbf{x} , and $\Omega \subset \mathbb{R}^n$ is an open, bounded domain with a well-behaved boundary $\partial\Omega$. In addition, $\mathbf{s} : \bar{\Omega} \rightarrow \mathbb{R}^m$ denotes the unknown latent quantity of interest that is governed by the PDE system of equation (2.1).

We proceed by approximating $\mathbf{s}(\mathbf{x})$ by a deep neural network $\mathbf{s}_{\theta}(\mathbf{x})$, where θ denotes all trainable parameters of the networks. Then, we can define the corresponding PDE residual as

$$\mathbf{r}_{\theta}(\mathbf{x}, t) := \frac{\partial}{\partial t} \mathbf{s}_{\theta}(\mathbf{x}, t) + \mathcal{N}_{\mathbf{x}}[\mathbf{s}_{\theta}(\mathbf{x}, t)], \quad (2.4)$$

where the partial derivatives of the neural network representation with respect to space and time coordinates can be readily computed to machine precision using forward or reverse mode automatic differentiation [34]. A physics-

informed neural network can be trained by minimizing the following composite loss function

$$\mathcal{L}(\boldsymbol{\theta}) = \lambda_r \mathcal{L}_r(\boldsymbol{\theta}) + \lambda_{bc} \mathcal{L}_{bc}(\boldsymbol{\theta}) + \lambda_{ic} \mathcal{L}_{ic}(\boldsymbol{\theta}), \quad (2.5)$$

where

$$\mathcal{L}_r(\boldsymbol{\theta}) = \frac{1}{N_r} \sum_{i=1}^{N_r} |\mathbf{r}_{\boldsymbol{\theta}}(\mathbf{x}_r^i, t_r^i)|^2, \quad (2.6)$$

$$\mathcal{L}_{bc}(\boldsymbol{\theta}) = \frac{1}{N_{bc}} \sum_{i=1}^{N_{bc}} |\mathbf{s}_{\boldsymbol{\theta}}(\mathbf{x}_{bc}^i, t_{bc}^i) - \mathbf{g}(\mathbf{x}_{bc}^i, t_{bc}^i)|^2, \quad (2.7)$$

$$\mathcal{L}_{ic}(\boldsymbol{\theta}) = \frac{1}{N_{ic}} \sum_{i=1}^{N_{ic}} |\mathbf{s}_{\boldsymbol{\theta}}(\mathbf{x}_{ic}^i, 0) - \mathbf{u}(\mathbf{x}_{ic}^i)|^2. \quad (2.8)$$

Here, N_r , N_{bc} and N_{ic} denote the batch-sizes of the "training data" $\{(\mathbf{x}_r^i, t_r^i), \mathbf{f}(\mathbf{x}_r^i, t_r^i)\}_{i=1}^{N_r}$, $\{(\mathbf{x}_{bc}^i, t_{bc}^i), \mathbf{g}(\mathbf{x}_{bc}^i, t_{bc}^i)\}_{i=1}^{N_{bc}}$ and $\{\mathbf{x}_{ic}^i, \mathbf{h}(\mathbf{x}_{ic}^i)\}_{i=1}^{N_{ic}}$, respectively, which are randomly sampled in the computational domain and the boundary at each iteration of a stochastic gradient descent algorithm. Moreover, the parameters $\{\lambda_r, \lambda_{bc}, \lambda_{ic}\}$ correspond to weight coefficients in the loss function that can effectively assign a different learning rate to each individual loss term. These weights may be user-specified or tuned automatically during network training [12, 13, 35].

Despite a series of promising results [22, 26, 27, 25], the original formulation of Raissi *et al.* [15] typically fails to handle long-time prediction tasks. To illustrate this, let us consider a simple gravity pendulum with damping governed by the following ODE system

$$\frac{ds_1}{dt} = s_2, \quad (2.9)$$

$$\frac{ds_2}{dt} = -\frac{b}{m} s_2 - \frac{g}{L} \sin(s_1), \quad (2.10)$$

for $t \in [0, T]$. The initial condition is given by $s_1(0) = s_2(0) = 1$. In this example, we take $m = L = 1$, $b = 0.05$ and $g = 9.81$. We are interested in using PINNs to solve this two-dimensional ODE system up to $T = 20$. To this end, we approximate the latent variables s_1, s_2 by a 5-layer fully-connected neural network $\mathbf{s}_{\boldsymbol{\theta}} = [s_{\boldsymbol{\theta}}^{(1)}, s_{\boldsymbol{\theta}}^{(2)}]$ with 100 units per hidden layer, and define the ODE residual as

$$\mathbf{r}_{\boldsymbol{\theta}}^{(1)}(t) = \frac{ds_{\boldsymbol{\theta}}^{(1)}(t)}{dt} - s_{\boldsymbol{\theta}}^{(2)}(t), \quad (2.11)$$

$$\mathbf{r}_{\boldsymbol{\theta}}^{(2)}(t) = \frac{ds_{\boldsymbol{\theta}}^{(2)}(t)}{dt} + \frac{b}{m} s_{\boldsymbol{\theta}}^{(2)}(t) - \frac{g}{L} \sin(s_{\boldsymbol{\theta}}^{(1)}(t)). \quad (2.12)$$

The corresponding PINNs loss function is given by

$$\mathcal{L}(\boldsymbol{\theta}) = \mathcal{L}_r(\boldsymbol{\theta}) + \mathcal{L}_{ic}(\boldsymbol{\theta}), \quad (2.13)$$

where

$$\mathcal{L}_r(\boldsymbol{\theta}) = \frac{1}{N_r} \sum_{i=1}^{N_r} \left[\left| \mathbf{r}_{\boldsymbol{\theta}}^{(1)}(t_r^i) \right|^2 + \left| \mathbf{r}_{\boldsymbol{\theta}}^{(2)}(t_r^i) \right|^2 \right], \quad (2.14)$$

$$\mathcal{L}_{ic}(\boldsymbol{\theta}) = \left| s_{\boldsymbol{\theta}}^{(1)}(0) - s_1(0) \right|^2 + \left| s_{\boldsymbol{\theta}}^{(2)}(0) - s_2(0) \right|^2. \quad (2.15)$$

We set $N_r = 10^4$, and all collocation points $\{t_r^i\}_{i=1}^{N_r}$ are randomly sampled in $[0, T]$ at each iteration during training. We train the network by minimizing the loss function (2.13) for 10^5 iterations of gradient descent using the Adam optimizer with default settings [36]. A comparison of the predicted solutions against their corresponding numerical estimation obtained with a conventional adaptive Runge-Kutta solver [3] is shown in Figure 1. It is clear that the PINN model predictions collapse to zero after $T = 10$, which suggests that PINNs may be incapable of yielding accurate solutions for long-time integration problems.

There are some reasons that may explain the poor predictions and model collapse. One could be saturated activation functions due to large values of the input coordinates. Another possible reason may be the inability of neural networks to approximate high-frequency and complex functions because of spectral bias [37]. Admittedly, recent work has provided

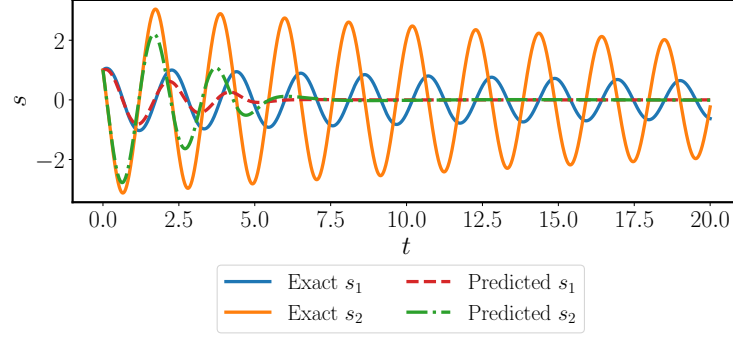


Figure 1: *Gravity Pendulum*: Predicted solution for $s_1(t)$ and $s_2(t)$ versus the corresponding reference solution. The result is obtained by training a conventional PINN (5 layers, 100 hidden units, tanh activations) for 10^5 iterations of gradient descent using the Adam optimizer. Evidently, the model predictions collapse after $t = 10$.

some remedies that can be directly applied to this case to improve model performance [38, 14, 39, 18]. For example, to avoid saturation of activations, one can normalize the inputs such that they lie in a reasonable range, although this trick will lead to very small coefficients in the ODE system, and, consequently, to a singular perturbation problem [40]. Other approaches include, but are not limited to, using Fourier feature embeddings [38, 14], as well as employing and training multiple individual networks in different temporal sub-domains [18, 39, 41]. The former typically requires some prior knowledge of the frequency content of the latent solution in order to properly initialize the model [14], while the latter approaches inevitably lead to a large computational cost. In the following sections, we present a simple yet effective strategy to solve long-time integration problems via physics-informed DeepONets [33].

3 Methods

3.1 A primer on physics-informed DeepONets

Recently, Lu *et. al.* [42] proposed deep operator networks (DeepONets), which aim to learn abstract nonlinear operators mapping functions between infinite-dimensional Banach spaces. In follow up work, Wang *et. al.* [33] developed physics-informed DeepONets, introducing an effective regularization mechanism for biasing the outputs of DeepONet models towards ensuring physical consistency. Here we present a brief overview of physics-informed DeepONets with a special focus on time-dependent PDEs (see equations (2.1) - (2.3)).

Let \mathcal{U}, \mathcal{S} be two separate Banach spaces. We are interested in learning the solution operator G from an initial condition $\mathbf{u} \in \mathcal{U}$ to the associated PDE solution $s(\mathbf{x}, t) \in \mathcal{S}$. To this end, we represent the solution map G by a DeepONet G_θ . As illustrated in Figure 2, the DeepONet architecture consists of two separate neural networks referred to as the "branch net" and "trunk net", respectively. The branch net takes the parameters \mathbf{s} as input and returns a features embedding $[b_1, b_2, \dots, b_q]^T \in \mathbb{R}^q$ as output, where $\mathbf{u} = [\mathbf{u}(\mathbf{x}_1), \mathbf{u}(\mathbf{x}_2), \dots, \mathbf{u}(\mathbf{x}_m)]$ represents a function $\mathbf{u} \in \mathcal{U}$ evaluated at a collection of fixed locations $\{\mathbf{x}_i\}_{i=1}^m \subset \Omega$. The trunk net takes the continuous coordinates (\mathbf{x}, t) as inputs, and outputs a features embedding $[t_1, t_2, \dots, t_q]^T \in \mathbb{R}^q$. The final output of the DeepONet is obtained by merging the outputs of the branch and trunk networks via a dot product. More specifically, a DeepONet G_θ prediction of an input function \mathbf{u} evaluated at (\mathbf{x}, t) can be expressed by

$$G_\theta(\mathbf{u})(\mathbf{x}, t) = \sum_{k=1}^q \underbrace{b_k(\mathbf{u}(\mathbf{x}_1), \mathbf{u}(\mathbf{x}_2), \dots, \mathbf{u}(\mathbf{x}_m))}_{\text{branch}} \underbrace{t_k(\mathbf{x}, t)}_{\text{trunk}}, \quad (3.1)$$

where θ denotes the collection of all trainable weights and biases in the branch and trunk networks. Note that the outputs of a DeepONet model are continuously differentiable with respect to the query points (\mathbf{x}, t) , thus allowing us to employ automatic differentiation [43, 34] to compute the associated PDE residual

$$\mathcal{R}_\theta[\mathbf{u}](\mathbf{x}, t) = \frac{\partial G_\theta(\mathbf{u})(\mathbf{x}, t)}{\partial t} + \mathcal{N}_\mathbf{x}[G_\theta(\mathbf{u})](\mathbf{x}, t). \quad (3.2)$$

Then, we can construct a physics-informed DeepONet by formulating the following loss function

$$\mathcal{L}(\theta) = \mathcal{L}_{\text{ic}}(\theta) + \mathcal{L}_{\text{bc}}(\theta) + \mathcal{L}_r(\theta), \quad (3.3)$$

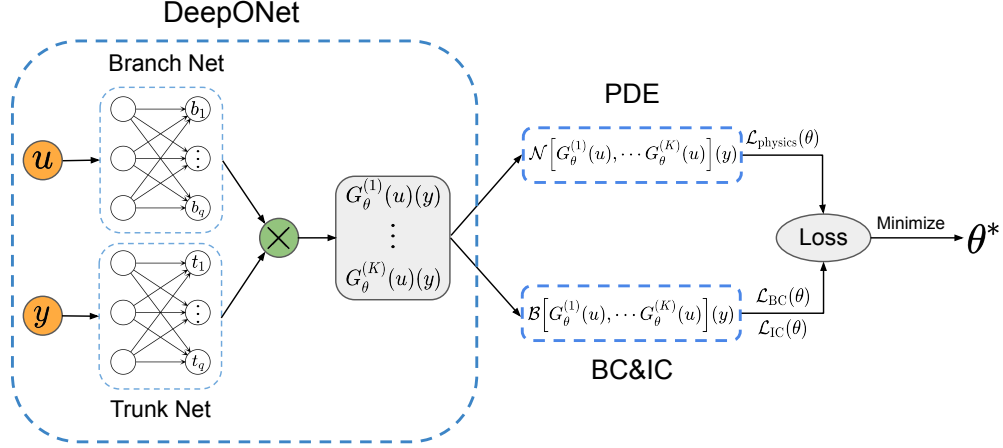


Figure 2: *Making DeepOnets physics-informed*: The DeepONet architecture [42] consists of two sub-networks, the branch net for extracting latent representations of input functions, and the trunk net for extracting latent representations of input coordinates at which the output functions are evaluated. A continuous and differentiable representation of the output functions is then obtained by merging the latent representations extracted by each sub-network via a dot product. Automatic differentiation can then be employed to formulate appropriate regularization mechanisms for biasing the DeepONet outputs to satisfy a given system of PDEs.

where

$$\mathcal{L}_{ic}(\theta) = \frac{1}{NP} \sum_{i=1}^N \sum_{j=1}^P \left| G_{\theta}(\mathbf{u}^{(i)})(\mathbf{x}_{ic,j}^{(i)}, 0) - \mathbf{u}^{(i)}(\mathbf{x}_{ic,j}^{(i)}) \right|^2 \quad (3.4)$$

$$\mathcal{L}_{bc}(\theta) = \frac{1}{NP} \sum_{i=1}^N \sum_{j=1}^P \left| G_{\theta}(\mathbf{u}^{(i)})(\mathbf{x}_{bc,j}^{(i)}, t_{bc,j}^{(i)}) - \mathbf{g}(\mathbf{x}_{bc,j}^{(i)}, t_{bc,j}^{(i)}) \right|^2, \quad (3.5)$$

$$\mathcal{L}_r(\theta) = \frac{1}{NQ} \sum_{i=1}^N \sum_{j=1}^Q \left| \mathcal{R}_{\theta}[\mathbf{u}^{(i)}](\mathbf{x}_{r,j}^{(i)}, t_{r,j}^{(i)}) \right|^2. \quad (3.6)$$

Here $\{\mathbf{u}^{(i)}\}_{i=1}^N$ denotes N separate input functions sampled from \mathcal{U} . For each $\mathbf{u}^{(i)}$, $\{(\mathbf{x}_{ic,j}^{(i)}, 0)\}_{j=1}^P$, $\{(\mathbf{x}_{bc,j}^{(i)}, t_{bc,j}^{(i)})\}_{j=1}^P$ are P locations sampled from $\Omega \times \{T = 0\}$ and $\partial\Omega \times [0, T]$ for enforcing the initial and boundary conditions, respectively. Besides, $\{(\mathbf{x}_{r,j}^{(i)}, t_{r,j}^{(i)})\}_{j=1}^Q$ is a set of collocation points sampled from the computational domain $\Omega \times [0, T]$ for penalizing the parametric PDE residual. In contrast to the fixed sensor locations of $\{\mathbf{x}_i\}_{i=1}^m$, we remark that the locations of $\{(\mathbf{x}_{ic,j}^{(i)}, 0)\}_{j=1}^P$, $\{(\mathbf{x}_{bc,j}^{(i)}, t_{bc,j}^{(i)})\}_{j=1}^P$ and $\{(\mathbf{x}_{r,j}^{(i)}, t_{r,j}^{(i)})\}_{j=1}^Q$ may vary across different input samples $\mathbf{u}^{(i)}$.

3.2 Long-time integration of evolution equations

In this section, we present our main contribution for solving time-dependent PDEs (2.1) - (2.3) involving long-time integration using physics-informed DeepONets. Instead of decomposing the temporal domain $[0, T]$ into many sub-domains and sequentially solving each short-time problem with an independent neural network, we train a single physics-informed DeepONet to learn the solution operator of the same PDE for a short time $t \in [0, \Delta t]$ subject to a distribution of initial conditions. Then we can obtain the inferred solution by recurrently replacing the initial condition with the model's prediction at $t = \Delta t$, and evaluating again the forward pass of the trained model. The details of the proposed strategy are summarized in Algorithm 1.

To introduce more technical details, let us revisit the example of gravity pendulum presented in section 2 and pursue its simulation up to $T = 100$. Before doing so, notice that the output of a vanilla DeepONet is a scalar, while the solution of the ODE system in equations (2.9) - (2.10) is a 2-dimensional vector. To resolve this issue, we modify the forward pass (3.1) such that the DeepONet output can be a vector. Specifically, suppose that a DeepONet outputs n different

Algorithm 1: Long-time integration of evolution equations with physics-informed DeepONets.

Suppose that G_θ is a trained physics-informed DeepONet that learned the solution operator of the time-dependent time PDE (2.1) - (2.3) for $t \in [0, \Delta t]$. Let $\{(\mathbf{x}_i, t_i)\}_{i=1}^P$ be a set of uniform grid points in $\Omega \times [0, \Delta t]$ and initialize the input function by $\mathbf{u}^0(\mathbf{x}) = \mathbf{u}(\mathbf{x})$ (the initial condition in equation (2.3)).

for $k = 1, \dots, N$ **do**

(a) Infer the solution by running the forward pass of the physics-informed DeepONet

$$\mathbf{s}^k(\mathbf{x}_i, t_i) = G_\theta(\mathbf{u}^{k-1})(\mathbf{x}_i, t_i), \quad \text{for } i = 1, 2, \dots, P. \quad (3.7)$$

(b) Update the input function by

$$\mathbf{u}^k(\mathbf{x}) = \mathbf{s}^k(\mathbf{x}, \Delta t) \quad (3.8)$$

end

The final predicted solution in the whole domain $\Omega \times [0, T]$ can be obtained by concatenating all the inferred solutions $\{\mathbf{s}^k\}_{k=1}^N$.

scalar functions. Then the forward pass of i -th function is given by

$$s_\theta^{(i)} = G_\theta^{(i)}(\mathbf{u})(\mathbf{x}, t) = \sum_{k=q_{i-1}+1}^{q_i} \underbrace{b_k(\mathbf{u}(\mathbf{x}_1), \mathbf{u}(\mathbf{x}_2), \dots, \mathbf{u}(\mathbf{x}_m))}_{\text{branch}} \underbrace{t_k(\mathbf{x}, t)}_{\text{trunk}} \quad (3.9)$$

for $i = 1, \dots, n$ where $0 = q_0 < q_1 < \dots < q_n = q$. For this 2D ODE, we take $n = 2$, $q = 200$ and $q_1 = 100$. Now we employ a DeepONet $G_\theta = [G_\theta^{(1)}, G_\theta^{(2)}]$ to represent the solution map from initial conditions to the associated solutions in $[0, 1]$, where both the branch and trunk networks are 8-layer fully-connected neural networks with 100 units per hidden layer. Similar to equation (2.11) - (2.12), we can define the ODE residual for the physics-informed DeepONet model as

$$\mathcal{R}_\theta^{(1)}[\mathbf{u}](t) = \frac{dG_\theta^{(1)}(\mathbf{u})(t)}{dt} - G_\theta^{(2)}(\mathbf{u})(t), \quad (3.10)$$

$$\mathcal{R}_\theta^{(2)}[\mathbf{u}](t) = \frac{dG_\theta^{(2)}(\mathbf{u})(t)}{dt} + \frac{b}{m} G_\theta^2(\mathbf{u})(t) - \frac{g}{L} \sin(G_\theta^{(1)}(\mathbf{u})(t)). \quad (3.11)$$

Then, the trainable parameters θ can be optimized by minimizing the following loss

$$\mathcal{L}(\theta) = \mathcal{L}_{\text{ic}}(\theta) + \mathcal{L}_r(\theta), \quad (3.12)$$

where

$$\mathcal{L}_{\text{ic}}(\theta) = \frac{1}{N} \sum_{i=1}^N \left[\left| G_\theta^{(1)}(\mathbf{u}^{(i)})(0) - u_1^{(i)} \right|^2 + \left| G_\theta^{(2)}(\mathbf{u}^{(i)})(0) - u_2^{(i)} \right|^2 \right] \quad (3.13)$$

$$\mathcal{L}_r(\theta) = \frac{1}{NQ} \sum_{i=1}^N \sum_{j=1}^Q \left[\left| \mathcal{R}_\theta^{(1)}[\mathbf{u}^{(i)}](t_j^{(i)}) \right|^2 + \left| \mathcal{R}_\theta^{(2)}[\mathbf{u}^{(i)}](t_j^{(i)}) \right|^2 \right]. \quad (3.14)$$

Here, $\mathbf{u}^{(i)} = [u_1^{(i)}, u_2^{(i)}]$ are the inputs of the branch network which denote the initial conditions. Moreover, for each i , $\{t_j^{(i)}\}_{j=1}^Q$ is a set of collocation points uniformly sampled from $[0, 1]$. In this example, we set $Q = 100$ and sample $N = 5 \times 10^4$ different initial conditions from a uniform distribution $\mathcal{U}(-3, 3)$. We train the physics-informed DeepONet for 3×10^5 iterations of gradient descent using Adam optimizer, and apply Algorithm 1 to the same initial condition as in the example presented in Figure 1. As shown in Figure 3, we observe that the model predictions are in good agreement with the exact solution. The resulting relative L^2 errors of $s^{(1)}$ and $s^{(2)}$ are 1.72% and 1.63%, respectively. It is worth emphasizing that the input function space \mathcal{U} should be large enough to cover as many potential states of the underlying ODE/PDE system as possible. Otherwise, the trained model may not generalize very well for out-of-distribution initial conditions, possibly leading to large errors or even erroneous predictions.

4 Results

To demonstrate the effectiveness of the proposed algorithm, we provide a series of comprehensive numerical studies for solving various long-time integration problems. Throughout all benchmarks, we will employ a modified fully-connected

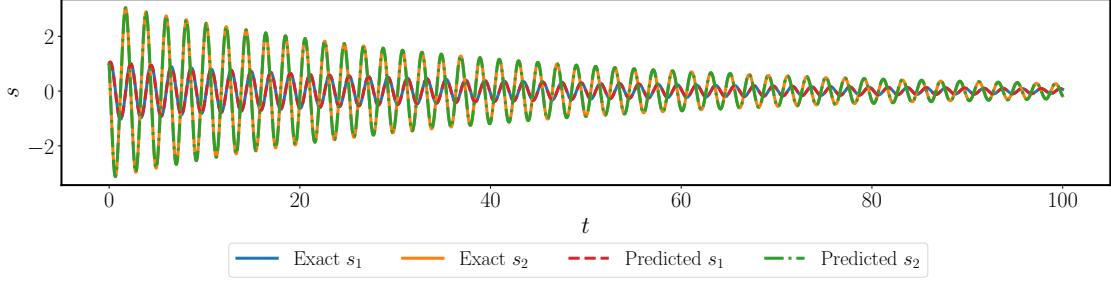


Figure 3: *Gravity Pendulum*: Predicted solution for $s_1(t)$ and $s_2(t)$ versus the corresponding reference solution. The result is obtained by applying Algorithm 1 to a trained a physics-informed DeepONet. The relative L^2 errors of s_1 and s_2 are 1.72% and 1.63%, respectively.

neural network architecture [12] which has been empirically proved to outperform the standard fully-connected neural network architectures [12, 33, 24]. The forward pass is defined by

$$U = \phi(XW^1 + b^1), \quad V = \phi(XW^2 + b^2) \quad (4.1)$$

$$H^{(1)} = \phi(XW^{z,1} + b^{z,1}) \quad (4.2)$$

$$Z^{(k)} = \phi(H^{(k)}W^{z,k} + b^{z,k}), \quad k = 1, \dots, L \quad (4.3)$$

$$H^{(k+1)} = (1 - Z^{(k)}) \odot U + Z^{(k)} \odot V, \quad k = 1, \dots, L \quad (4.4)$$

$$f_{\theta}(x) = H^{(L+1)}W + b, \quad (4.5)$$

where X denotes the network inputs, and \odot denotes element-wise multiplication. The parameters of this model are essentially the same as in conventional fully-connected architectures, with the addition of the weights and biases used by the two transformer sub-networks, i.e.,

$$\theta = \{W^1, b^1, W^2, b^2, (W^{z,l}, b^{z,l})_{l=1}^L, W, b\} \quad (4.6)$$

In all cases we employ hyperbolic tangent activation functions (Tanh) and initialize all trainable parameters using the Glorot normal scheme [44]. Physics-informed DeepONet models are trained via mini-batch gradient descent with a batch-size of 10,000 using the Adam optimizer with default settings [36], and an exponential learning rate decay with a decay-rate of 0.9 every 5,000 iterations. In this work, we tuned these hyper-parameters manually, without attempting to find the absolute best hyper-parameter setting. This process can be automated in the future leveraging effective techniques for meta-learning and hyper-parameter optimization [45]. Additional details related to performance metrics, computational cost, hyper-parameters and training details are discussed in the Appendix. All results presented in this section can be reproduced using open-source code that will be made publicly available at <https://github.com/PredictiveIntelligenceLab/Long-time-Integration-PI-DeepONets>.

4.1 Inhomogeneous ODEs

As our first example, we start with a simple benchmark to illustrate how to generalize Algorithm 1 to inhomogeneous differential equations. Particularly, we consider a 1D ODE of the form

$$\frac{ds}{dt} = \cos(t), \quad t \in [0, T], \quad (4.7)$$

$$s(0) = 0. \quad (4.8)$$

The objective is to use Algorithm 1 to learn the ODE solution for $T = 10^3$. However, one may note that the proposed algorithm cannot be directly applied to this problem because of the forcing term. For example, assume that G_{θ} is a trained physics-informed DeepONet that approximates the solution operator from the initial condition to the associated solution of the ODE (4.7) for $t \in [0, 1]$ and $\tilde{s}(t)$ is an inferred solution corresponding to some initial condition. To obtain the solution in $[1, 2]$, the trained DeepONet is required to yield the predicted solution governed by the following ODE

$$\begin{aligned} \frac{ds}{dt} &= \cos(t+1), \quad t \in [0, 1], \\ s(0) &= \tilde{s}(1), \end{aligned}$$

which is impossible because the trained model would be designing to work with a fixed forcing term. Fortunately, one can easily overcome this technical difficulty by solving the following parametric ODE

$$\frac{ds}{dt} = u(t), \quad t \in [0, \Delta t] \quad (4.9)$$

$$s(0) = u_0 \quad (4.10)$$

where both the initial condition and the forcing term can be considered as random inputs.

To represent the solution map of the above parametric ODE with a DeepONet G_{θ} , we employ a single trunk network for extracting latent representations of input coordinates, but two separate branch networks for representing the initial condition and the forcing term, respectively. The final output of the modified DeepONet architecture can be then obtained as

$$G_{\theta}(\mathbf{u}, u_0)(t) = \sum_{k=1}^q \underbrace{b_k^{(1)}(u(t_1), u(t_2), \dots, u(t_m))}_{\text{branch I}} \cdot \underbrace{b_k^{(2)}(u_0)}_{\text{branch II}} \cdot \underbrace{t_k(t)}_{\text{trunk}}, \quad (4.11)$$

where $\{b_k^{(1)}\}_{k=1}^q, \{b_k^{(2)}\}_{k=1}^q$ are outputs of two branch networks, respectively, and u_0 denotes the input initial condition. Also, $\mathbf{u} = [u(t_1), u(t_2), \dots, u(t_m)]$ represents the input forcing term evaluated at a set of fixed sensors $\{t_k\}_{k=1}^m \subset [0, \Delta t]$. In this example, we take $\Delta t = 1, m = 100$ and then $\{t_i\}_{i=1}^m$ are equi-spaced grid points in $[0, 1]$. Besides, all neural networks are 7-layer modified fully-connected neural networks (see equations (4.1)-(4.5)) with 100 units per hidden layer. The resulting physics-informed DeepONet can be trained by minimizing the following loss

$$\mathcal{L}(\theta) = \mathcal{L}_{\text{ic}}(\theta) + \mathcal{L}_r(\theta), \quad (4.12)$$

where

$$\mathcal{L}_{\text{ic}}(\theta) = \frac{1}{N} \sum_{i=1}^N \left| G_{\theta}(\mathbf{u}^{(i)}, u_0^{(i)})(0) - u_0^{(i)} \right|^2, \quad (4.13)$$

$$\mathcal{L}_r(\theta) = \frac{1}{NQ} \sum_{i=1}^N \sum_{j=1}^Q \left| G_{\theta}(\mathbf{u}^{(i)}, u_0^{(i)})(t_j^{(i)}) - u^{(i)}(t_j^{(i)}) \right|^2. \quad (4.14)$$

We generate "training data" by randomly sampling $N = 5 \times 10^4$ inputs $\{\mathbf{u}^{(i)}\}_{i=1}^N, \{u_0^{(i)}\}_{i=1}^N$ from a Gaussian random field (GRF) with a length scale of $l = 0.5$ and a uniform distribution $\mathcal{U}(-2, 2)$, respectively. For each paired input sample $(\mathbf{u}^{(i)}, u_0^{(i)})$, the collocation points $\{t_j^{(i)}\}_{j=1}^Q$ are uniformly sampled in the unit interval with $Q = 100$.

Figure 4 shows the inferred solution of the ODE system (4.7)-(4.8) obtained by applying Algorithm 1 to a physics-informed DeepONet that was trained for 2×10^5 gradient descent iterations via the Adam optimizer [36]. It can be observed that the model prediction achieves an excellent agreement with the exact solution as the resulting relative L^2 error over the whole time-domain is 0.84%. More interestingly, Algorithm 1 also performs very well for different initial conditions sampled from a different function space than the one used to train the model ($\mathcal{U}(-3, 3)$). To illustrate this, we randomly sample $N = 100$ different u_0 from a uniform distribution $\mathcal{U}(-\frac{1}{2}, \frac{1}{2})$ and obtain the inferred solution using the proposed algorithm. The relative L^2 error at the final time T averaged across all examples in the test data-set is displayed in Figure 5. One can see that all the inferred solutions keep almost the same accuracy ($\sim 0.5\%$) up to $T = 100$, while the approximation errors tend to accumulate as time T increases. Additional visualizations for different input samples are provided in Appendix Figure 16.

4.2 Stiff chemical kinetics

Our next example aims to demonstrate the capability of the proposed algorithm to perform long-time integration of stiff ODEs, which are generally hard to solve by conventional PINNs [46], as well as classical numerical methods [47, 3]. To this end, we consider a classical stiff chemical kinetics problem describing the kinetics of an autocatalytic reaction [48, 47]

$$\frac{ds_1}{dt} = -k_1 s_1 + k_3 s_2 s_3, \quad (4.15)$$

$$\frac{ds_2}{dt} = k_1 s_1 - k_2 s_2^2 - k_3 s_2 s_3, \quad (4.16)$$

$$\frac{ds_3}{dt} = k_2 s_2^2, \quad (4.17)$$

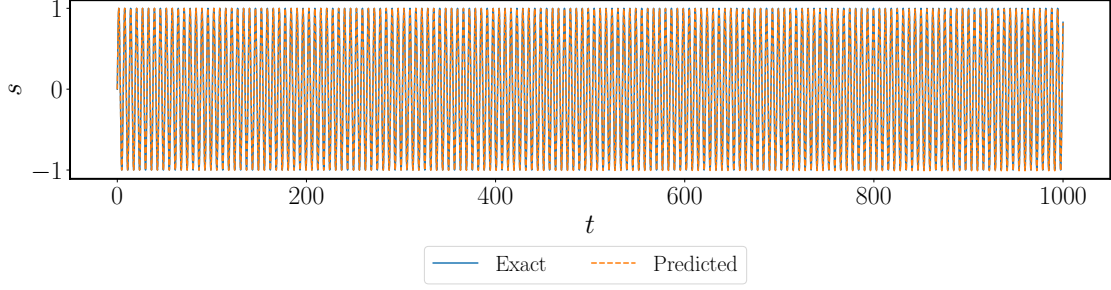


Figure 4: *Inhomogeneous ODE*: Exact solution versus the predicted solution of a trained physics-informed DeepONet using Algorithm 1 to integrate the ODE system of equations (4.7) - (4.8) up to $T = 1000$. The relative L^2 error is 0.84%.

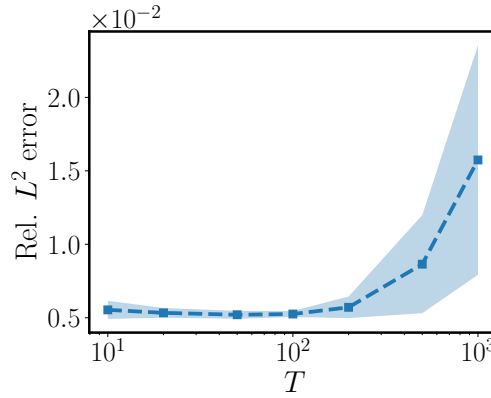


Figure 5: *linear ODE*: Relative L^2 prediction error of a physics-informed DeepONet as a function of the final time T , averaged over 100 different examples in the test data-set.

with the initial condition

$$s_1(0) = 1, \quad s_2(0) = s_3(0) = 0, \quad (4.18)$$

where s_1, s_2, s_3 denote the concentrations of different chemical species, while the reaction rate constants are $k_1 = 0.04, k_2 = 3 \times 10^4, k_3 = 10^7$. It worth pointing out that the different species have very different reaction timescales, especially for s_2 , which consequently results in a very stiff system.

We proceed by employing a physics-informed DeepONet \mathbf{G}_θ to represent the solution operator G mapping the initial condition $\mathbf{u} \in \mathbb{R}^3$ to the solution of the kinetic system in time interval $[0, 1]$ (i.e., $\Delta t = 1$). Since the ODE system has three variables, the forward pass of the DeepONet is given by equation (3.9) where we take $i = 3$ and $[q_0, q_1, q_2, q_3] = [0, 100, 200, 300]$. Accordingly, the ODE residuals are defined by

$$\mathcal{R}_\theta^{(1)}[\mathbf{u}](t) = \frac{dG_\theta^{(1)}(\mathbf{u})(t)}{dt} + k_1 G_\theta^{(1)}(\mathbf{u})(t) - k_3 G_\theta^{(2)}(\mathbf{u})(t) G_\theta^{(3)}(\mathbf{u})(t), \quad (4.19)$$

$$\mathcal{R}_\theta^{(2)}[\mathbf{u}](t) = \frac{dG_\theta^{(2)}(\mathbf{u})(t)}{dt} - k_1 G_\theta^{(1)}(\mathbf{u})(t) + k_2 [G_\theta^{(2)}(\mathbf{u})(t)]^2 + k_3 G_\theta^{(2)}(\mathbf{u})(t) G_\theta^{(3)}(\mathbf{u})(t), \quad (4.20)$$

$$\mathcal{R}_\theta^{(3)}[\mathbf{u}](t) = \frac{dG_\theta^{(3)}(\mathbf{u})(t)}{dt} - k_2 [G_\theta^{(2)}(\mathbf{u})(t)]^2, \quad (4.21)$$

where $\mathbf{G}_\theta = [G_\theta^{(1)}, G_\theta^{(2)}, G_\theta^{(3)}]$ represents the three species $[s_1, s_2, s_3]$ in the kinetic system, and $\mathbf{u} = [u_1, u_2, u_3]$ denotes the initial concentration for each state variable. This allows us to formulate the physics-informed loss function

$$\mathcal{L}(\theta) = \mathcal{L}_{\text{ic}}(\theta) + \mathcal{L}_r(\theta), \quad (4.22)$$

where

$$\mathcal{L}_{\text{ic}}(\boldsymbol{\theta}) = \sum_{k=1}^3 \lambda_k \mathcal{L}_{\text{ic}}^{(k)}(\boldsymbol{\theta}) = \sum_{k=1}^3 \lambda_k \left[\frac{1}{N} \sum_{i=1}^N \left| G_{\boldsymbol{\theta}}^{(k)}(\mathbf{u}^{(i)})(0) - u_k^{(i)} \right|^2 \right], \quad (4.23)$$

$$\mathcal{L}_r(\boldsymbol{\theta}) = \sum_{k=1}^3 \mathcal{L}_r^{(k)}(\boldsymbol{\theta}) = \sum_{k=1}^3 \left[\frac{1}{NQ} \sum_{i=1}^N \sum_{j=1}^Q \left| \mathcal{R}_{\boldsymbol{\theta}}^{(k)}[\mathbf{u}^{(i)}](t_j^{(i)}) \right|^2 \right]. \quad (4.24)$$

In this example, the branch and trunk networks parametrizing $G_{\boldsymbol{\theta}}$ are two 7-layer modified fully-connected neural networks with 100 neurons per hidden layer (see equations (4.1)-(4.5)). The model is trained on a data-set created by randomly sampling $N = 5 \times 10^4$ initial states $\{\mathbf{u}^{(i)}\}_{i=1}^N = \{[u_1^{(i)}, u_2^{(i)}, u_3^{(i)}]\}_{i=1}^N$, where $u_1^{(i)}, u_3^{(i)} \sim \mathcal{U}(0, 1)$, and $u_2^{(i)} \sim \mathcal{U}(0, 10^{-4})$, for all i . For each input sample \mathbf{u}^i we have $Q = 10^3$, and $\{t_j^{(i)}\}_{j=1}^Q$ are collocation points sampled from $\mathcal{U}(0, 1)$. Furthermore, because the species s_2 is typically about four order of magnitudes smaller than s_1 and s_3 , we manually re-scale the range of $G_{\boldsymbol{\theta}}^{(2)}$ by multiplying it by 10^{-4} , and set $[\lambda_1, \lambda_2, \lambda_3] = [1, 10^6, 1]$ to the corresponding imbalance between the different loss functions. To generate the test data-set, we randomly sample 100 initial conditions, and obtain the corresponding numerical solutions in $[0, 500]$ by integrating the ODE using the Radau scheme [49].

We train the physics-informed DeepONet by minimizing the loss of equation (4.22) for 4×10^5 gradient descent iterations using the Adam optimizer. The inferred solution obtained using the trained model subject to the initial condition (4.18) is presented in the top panel of Figure 6, from which we can observe an excellent agreement between the model inference and the ground truth with relative L^2 errors of 0.38%, 0.56%, 0.64% for s_1, s_2, s_3 , respectively. Some representative visualizations for different initial conditions are shown in Appendix Figure 18. Moreover, the relative L^2 error of the model predictions, averaged over all 100 examples in the test data-set, is visualized in Figure 7. From these figures, one may conclude that the trained model is capable of yielding accurate long-time predictions for different initial conditions.

To demonstrate the necessity of assigning weights to the different terms in the physics-informed loss function, we train the same model without any weights under exactly the same hyper-parameter settings, and the result is summarized in the bottom panel of Figure 6. It is evident that the un-scaled physics-informed DeepONet fails to learn the correct solution even on a unit interval, let alone long-time integration. These observations are consistent with the findings reported in [12, 13, 33], highly suggesting that rescaling the network outputs and the loss functions is a prerequisite for achieving good predictive accuracy, especially for problems that exhibit stiff and multi-scale behavior. Although here we manually assign weights assuming some prior knowledge of the underlying ODE model form, it must be emphasized that such a manual approach is time-consuming or even impractical for many realistic scenarios involving high-dimensional state spaces, multi-physics, complicated loss functions, etc. Hence, we point out that there is an urgent need to understand the training dynamics of physics-informed DeepONets and develop effective training algorithms that can automatically balance the interplay between different terms in the corresponding loss functions.

Once trained, the model can be rapidly queried to return prediction at short-time intervals. Each query typically takes $\mathcal{O}(10^{-3}\text{ms})$ on a single Nvidia V100 GPU. Constructing the global PDE/ODE solution in large temporal domains using Algorithm 1 requires $N \sim \mathcal{O}(10) - \mathcal{O}(10^3)$ evaluations of the trained model, typically leading to a total inference time of $\sim \mathcal{O}(10^{-2})$ sec for a given initial condition. Multiple initial conditions can also be simulated at once, as our JAX [50] implementation is trivial vectorized and parallelized on GPU hardware. As demonstrated in Figure 7, the proposed framework can perform long-time integration of more than 1,000 initial conditions in $\mathcal{O}(1)$ second, yielding a $\sim 10\text{x}-50\text{x}$ speedup compared to a traditional numerical solver. Unlike traditional numerical solvers that are heavily specialized to a specific type of dynamic behavior, this cost remains nearly constant for all examples considered in this work, regardless of the ODE/PDE system that is simulated, as it merely amounts to the cost associated with evaluating the forward pass of the trained DeepONet model.

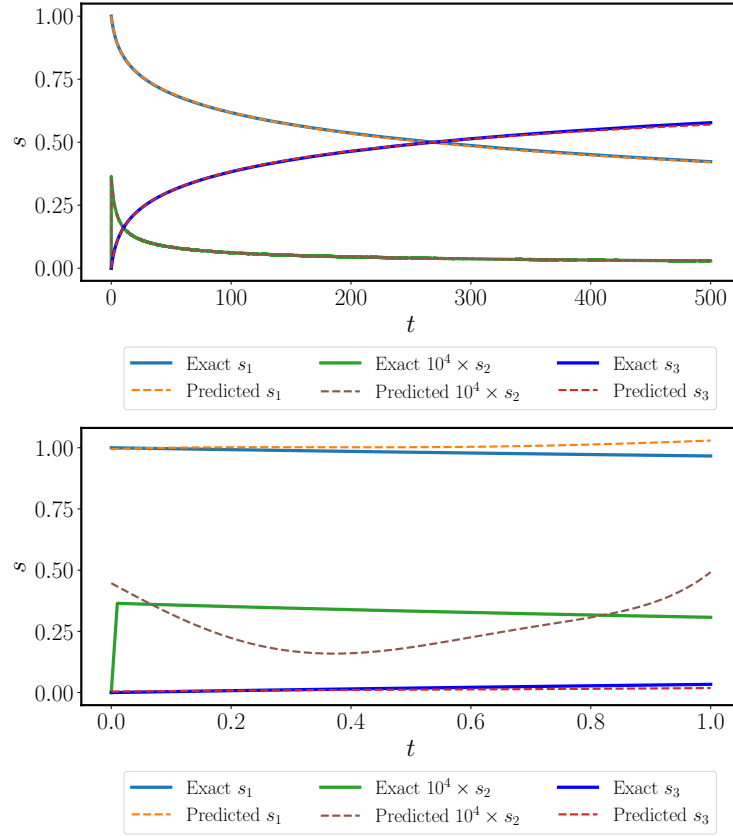


Figure 6: *Stiff chemical kinetics*: *Top*: Reference solution versus the prediction of a trained scaled physics-informed DeepONet using Algorithm 1 for integrating the ODE system of equations (4.15) - (4.18) up to $T = 500$. The relative L^2 errors for s_1, s_2, s_3 are 0.38%, 0.56%, 0.64%, respectively. *Bottom*: Reference solution versus the prediction of a trained un-scaled physics-informed DeepONet. The relative L^2 errors for s_1, s_2, s_3 are 3.05%, 37.01%, 41.93%, respectively. We can observe that the trained model fails to yield accurate predictions even for a short-time interval corresponding to $T = 1$.

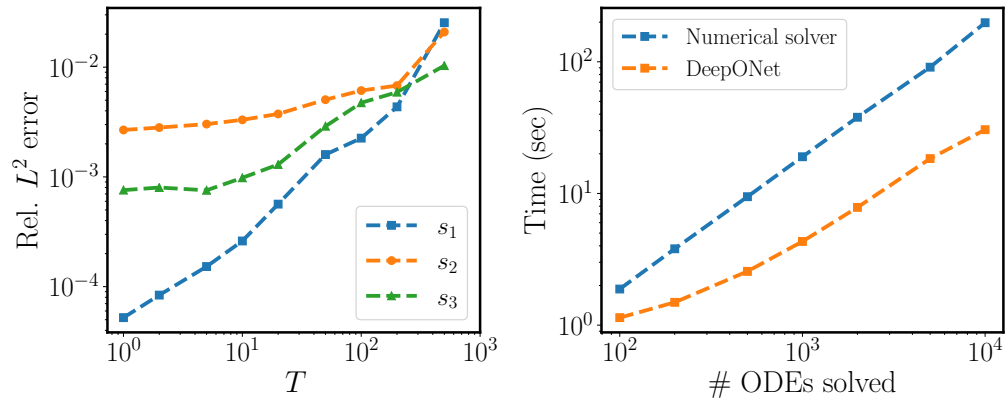


Figure 7: *Stiff chemical kinetics*: *Left*: Relative L^2 prediction error of a trained physics-informed DeepONet as a function of the final prediction time T , averaged over 100 different examples in the test data-set. *Right*: Computational cost (sec) for performing inference with a trained physics-informed DeepONet model versus the time taken for solving the ODE with a conventional Runge-Kutta scheme [49].

4.3 Wave propagation

In the numerical examples presented so far we mainly focus on ODEs. To highlight the ability of the proposed algorithm to handle long-time integration problems for PDEs, we begin by considering the 1D wave equation

$$\frac{\partial^2 s}{\partial t^2} = c^2 \frac{\partial^2 s}{\partial x^2}, \quad (x, t) \in [0, 1] \times [0, T], \quad (4.25)$$

$$s(0, t) = s(1, t) = 0, \quad t \in [0, T], \quad (4.26)$$

$$s(x, 0) = \sin(\pi x), \quad x \in [0, 1], \quad (4.27)$$

$$\frac{\partial s}{\partial t}(x, 0) = 0, \quad (4.28)$$

where we take $c = 1$ and $T = 100$. The exact solution is given by

$$s(x, t) = \sin(\pi x) \cos(c\pi t). \quad (4.29)$$

To solve this problem, we parametrize the initial condition by a Gaussian random field with a length scale $l = 0.5$, and use a DeepONet G_θ to represent the solution map from initial conditions to the associated PDE solutions. Here, the branch and trunk networks are 5-layer modified fully-connected neural networks (see equations (4.1)-(4.5)) with 200 units per hidden layer. The parameters of the physics-informed DeepONet can be trained by minimizing the following loss function

$$\mathcal{L}(\theta) = \mathcal{L}_{\text{ic}}(\theta) + \mathcal{L}_{\text{bc}}(\theta) + \mathcal{L}_r(\theta), \quad (4.30)$$

where

$$\mathcal{L}_{\text{ic}}(\theta) = \frac{1}{NP} \sum_{i=1}^N \sum_{j=1}^P \left[\left| G_\theta(\mathbf{u}^{(i)})(x_{\text{ic},j}^{(i)}, 0) - u^{(i)}(x_{\text{ic},j}^{(i)}) \right|^2 + \left| \frac{\partial G_\theta(\mathbf{u}^{(i)})}{\partial t}(x_{\text{ic},j}^{(i)}, 0) \right|^2 \right], \quad (4.31)$$

$$\mathcal{L}_{\text{bc}}(\theta) = \frac{1}{NP} \sum_{i=1}^N \sum_{j=1}^P \left[\left| G_\theta(\mathbf{u}^{(i)})(0, t_{\text{bc},j}^{(i)}) \right|^2 + \left| G_\theta(\mathbf{u}^{(i)})(1, t_{\text{bc},j}^{(i)}) \right|^2 \right], \quad (4.32)$$

$$\mathcal{L}_r(\theta) = \frac{1}{NQ} \sum_{i=1}^N \sum_{j=1}^Q \left| \frac{\partial^2 G_\theta(\mathbf{u}^{(i)})}{\partial t^2}(x_{r,j}^{(i)}, t_{r,j}^{(i)}) - c^2 \frac{\partial^2 G_\theta(\mathbf{u}^{(i)})}{\partial x^2}(x_{r,j}^{(i)}, t_{r,j}^{(i)}) \right|^2. \quad (4.33)$$

Here, we take $\Delta t = 1$, $N = 10^4$, $m = P = 100$ and $Q = 200$. In particular, for every input sample $\mathbf{u}^{(i)}$, $\{x_{\text{ic},j}^{(i)}\}_{j=1}^P$, $\{t_{\text{bc},j}^{(i)}\}_{j=1}^P$ and $\{x_{r,j}^{(i)}, t_{r,j}^{(i)}\}_{j=1}^Q$ are uniformly sampled in the computational domain $[0, 1] \times [0, 1]$ for enforcing the initial/boundary conditions and the PDE residual, respectively. We train the physics-informed DeepONet for 2×10^5 iterations of gradient descent using the Adam optimizer. A comparison of the long-time prediction against the ground truth is shown in Figure 8. We can observe a good agreement between the predicted and the exact solution, yielding a relative error of $1.57e - 02$ in the relative L^2 norm.

4.4 Diffusion-reaction dynamics

Next, we present a study on the effect of Δt in Algorithm 1 by solving a long-time integration problem involving non-linear diffusion-reaction dynamics, as described by the following PDE system

$$\frac{\partial s}{\partial t} = D \frac{\partial^2 s}{\partial x^2} + ks^2, \quad (x, t) \in (0, 1] \times (0, T], \quad (4.34)$$

$$s(x, 0) = u(x), \quad x \in [0, 1] \quad (4.35)$$

$$s(0, t) = s(1, t) = 0, \quad t \in [0, T], \quad (4.36)$$

where $T = 50$, $D = 0.001$ is the diffusion coefficient, and $k = 0.001$ is the reaction rate. According to Algorithm 1, it suffices to learn the solution operator that maps the initial condition to the associated PDE solution in $[0, \Delta t]$. To this end, we approximate the operator by a DeepONet G_θ where the branch net and the trunk network are 5-layer modified fully-connected neural network (see equations (4.1)-(4.5)) with 100 units per hidden layer. The physics-informed loss function is given by

$$\mathcal{L}(\theta) = \mathcal{L}_{\text{ic}}(\theta) + \mathcal{L}_{\text{bc}}(\theta) + \mathcal{L}_r(\theta), \quad (4.37)$$

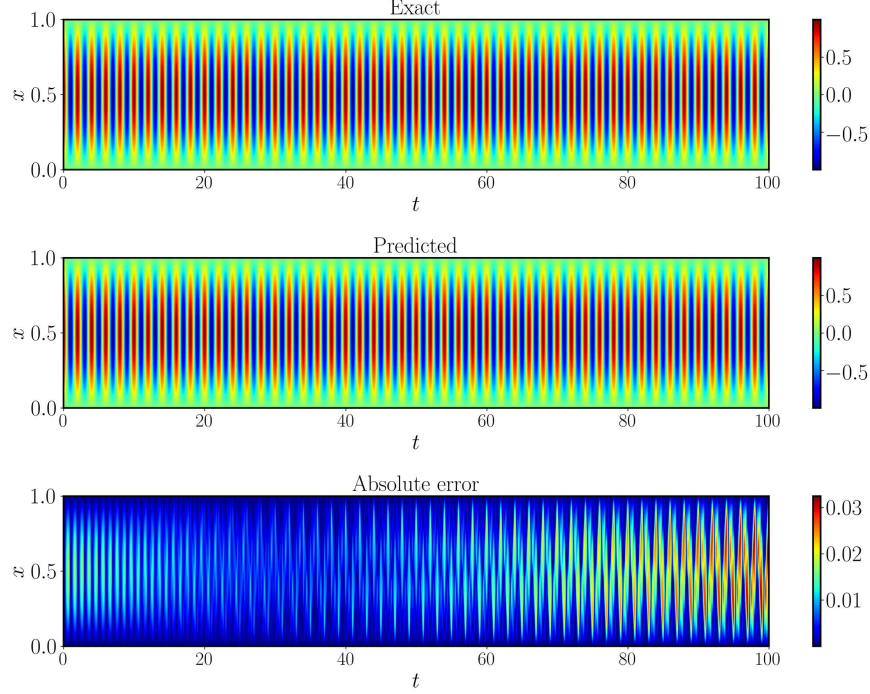


Figure 8: *Wave propagation*: Comparison between the exact and the predicted solution of a trained physics-informed DeepONet using Algorithm 1 for integrating the PDE (4.25) - (4.28) up to $T = 100$. The relative L^2 error is 1.57%.

where

$$\mathcal{L}_{\text{ic}}(\boldsymbol{\theta}) = \frac{1}{NP} \sum_{i=1}^N \sum_{j=1}^P \left| G_{\boldsymbol{\theta}}(\mathbf{u}^{(i)})(x_{\text{ic},j}^{(i)}, 0) - u^{(i)}(x_{\text{ic},j}^{(i)}) \right|^2, \quad (4.38)$$

$$\mathcal{L}_{\text{bc}}(\boldsymbol{\theta}) = \frac{1}{NP} \sum_{i=1}^N \sum_{j=1}^P \left[\left| G_{\boldsymbol{\theta}}(\mathbf{u}^{(i)})(0, t_{\text{bc},j}^{(i)}) \right|^2 + \left| G_{\boldsymbol{\theta}}(\mathbf{u}^{(i)})(1, t_{\text{bc},j}^{(i)}) \right|^2 \right], \quad (4.39)$$

$$\mathcal{L}_r(\boldsymbol{\theta}) = \frac{1}{NQ} \sum_{i=1}^N \sum_{j=1}^Q \left| \frac{\partial G_{\boldsymbol{\theta}}(\mathbf{u}^{(i)})}{\partial t}(x_{r,j}^{(i)}, t_{r,j}^{(i)}) - D \frac{\partial^2 G_{\boldsymbol{\theta}}(\mathbf{u}^{(i)})}{\partial x^2}(x_{r,j}^{(i)}, t_{r,j}^{(i)}) - k G_{\boldsymbol{\theta}}^2(\mathbf{u}^{(i)})(x_{r,j}^{(i)}, t_{r,j}^{(i)}) \right|. \quad (4.40)$$

Here, $\mathbf{u}^{(i)}$ denotes initial conditions randomly sampled from a GRF with a length scale of $l = 0.2$, and for each input sample, $\{x_{\text{ic},j}^{(i)}\}_{j=1}^P$, $\{t_{\text{bc},j}^{(i)}\}_{j=1}^P$ and $\{x_{r,j}^{(i)}, t_{r,j}^{(i)}\}_{j=1}^Q$ are uniformly sampled in the computational domain $[0, 1] \times [0, \Delta t]$. In this example, we take $N = 10^4$ and $m = P = Q = 100$. To generate the test data-set, we sample $N = 100$ input functions $u(x)$ from the same GRF and solve the diffusion-reaction system in $[0, 1] \times [0, T]$ by a second-order implicit finite difference method.

For different Δt , we train the physics-informed DeepONet for 2×10^5 iterations under exactly the same hyper-parameter settings. Figure 9 shows the relative L^2 prediction errors of the trained models averaged over all examples in the test data-set. A key observation is that our approach is relatively robust against the choice of the time step size Δt , while trained model corresponding to $\Delta t = 1$ seems to yield the best predictive accuracy. Moreover, the predicted solution of the best trained model for one representative input sample is shown in Figure 10. One can see that the predictions achieves an excellent agreement with the corresponding numerical estimations. The resulting relative L^2 error is 0.67%. Additional representative results corresponding to different initial conditions can be found in the Appendix Figure 21, which further verifies our conclusion.

4.5 Korteweg–De Vries equation

In our last example we would like to emphasize the effectiveness of physics-informed DeepONets in integrating observational data and governing evolution equations in a data-efficient manner. To this end, we pursue the long-time

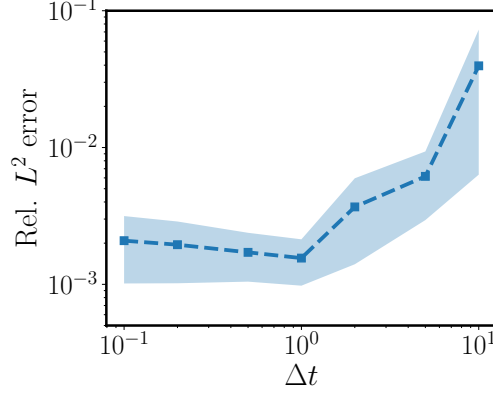


Figure 9: *Diffusion-reaction dynamics*: Relative L^2 prediction errors of trained physics-informed DeepONets for different $\Delta t \in [0.1, 10]$, averaged over 100 different examples in the test data-set.

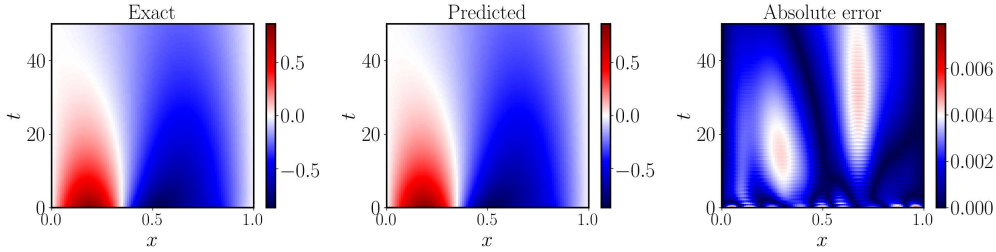


Figure 10: *Diffusion-reaction dynamics*: Reference solution versus the predicted solution of a trained physics-informed DeepONet using Algorithm 1 for a representative input sample in the test data-set. The relative L^2 prediction error is 0.67%.

prediction of traveling solitons governed by the Korteweg–De Vries (KDV) equation, assuming that, instead of boundary conditions for the latent solution, only some sparse observations in a short-time interval are available. Specifically, we set $\epsilon = 1.2 \times 10^{-1}$ and $\mu = 8 \times 10^{-4}$ and consider the following PDE system

$$\frac{\partial s}{\partial t} + \epsilon \frac{\partial s}{\partial x} s + \mu \frac{\partial^3 s}{\partial x^3} = 0, \quad x \in [0, 5], \quad (4.41)$$

subject to the initial condition $s(x, 0) = u(x)$. For single solitons, the exact solution can be derived as [51]

$$s(x, t) = \frac{c}{2} \operatorname{sech}^2 \left[\frac{\sqrt{c}}{2} \left(5x - \frac{1}{10} ct - a \right) \right] \quad (4.42)$$

where c denotes the travel speed of a wave and a determines the initial wave position in the physical domain. It is well-known that the KDV equation is one of the most important non-linear PDEs, originally derived to model shallow water waves and then used to describe a diversity of important finite amplitude dispersive wave phenomena in physics, such as acoustic waves in a harmonic crystal and ion-acoustic waves in plasmas [52]. Using Algorithm 1, the problem can be reduced to learning the solution operator G mapping initial conditions to the corresponding PDE solutions in $[0, \Delta t]$.

We proceed by approximating G with a DeepONet G_θ , where both the branch and trunk networks are 7-layer modified fully-connected neural networks (see equations (4.1)-(4.5)) with 200 neurons per hidden layer. This allows us to define the corresponding PDE residual

$$\mathcal{R}[\mathbf{u}](x, t) = \frac{\partial G_\theta(\mathbf{u})}{\partial t}(x, t) + \epsilon G_\theta(\mathbf{u})(x, t) \frac{\partial G_\theta(\mathbf{u})}{\partial x}(x, t) + \mu \frac{\partial^3 G_\theta(\mathbf{u})}{\partial x^3}(x, t), \quad (4.43)$$

used to formulate the following loss function

$$\mathcal{L}(\theta) = \mathcal{L}_{\text{data}}(\theta) + \mathcal{L}_{\text{physics}}(\theta), \quad (4.44)$$

where

$$\mathcal{L}_{\text{data}}(\boldsymbol{\theta}) = \frac{1}{NP} \sum_{i=1}^N \sum_{j=1}^P \left| G_{\boldsymbol{\theta}}(\mathbf{u}^{(i)})(x_{s,j}^{(i)}, t_{s,j}^{(i)}) - s^{(i)}(x_{s,j}^{(i)}, t_{s,j}^{(i)}) \right|,$$

$$\mathcal{L}_{\text{physics}}(\boldsymbol{\theta}) = \frac{1}{NQ} \sum_{i=1}^N \sum_{j=1}^Q \left| \mathcal{R}[\mathbf{u}^{(i)}](x_j^{(i)}, t_j^{(i)}) - s^{(i)}(x_{r,j}^{(i)}, t_{r,j}^{(i)}) \right|.$$

Here, $\mathbf{u}^{(i)} = [u^{(i)}(x_1), u^{(i)}(x_2), \dots, u^{(i)}(x_m)]$ denotes the initial conditions evaluated at a set of fixed sensor locations $\{x_i\}_{i=1}^m$, and $s^{(i)}$ is the associated PDE solution corresponding to each $u^{(i)}$. For every i , $\{(x_{s,j}^{(i)}, t_{s,j}^{(i)}), s^{(i)}(x_{s,j}^{(i)}, t_{s,j}^{(i)})\}_{j=1}^P$ are available solution measurements, while $\{(x_j^{(i)}, t_j^{(i)}) - s^{(i)}(x_{r,j}^{(i)}, t_{r,j}^{(i)})\}_{j=1}^Q$ is a set of collocation points randomly sampled in the computational domain $[0, 5] \times [0, \Delta t]$ for imposing the PDE constraint. To obtain a set of training data, we sample pairs (a, c) where $a \sim \mathcal{U}(0, 5)$, $b \sim \mathcal{U}(0, 1)$, and randomly selecting P observations of the exact solution $s(x, t)$ using equation (4.42). In this example, we set $N = 5 \times 10^3$, $\Delta t = 10$ and $m = P = Q = 200$.

We train the proposed physics-informed DeepONet using the Adam optimizer for 2×10^5 iterations, and then apply Algorithm 1 to the initial condition with $a = 1$, $c = 3/2$, i.e

$$s(x, 0) = \frac{3}{4} \operatorname{sech}^2 \left[\frac{\sqrt{3/2}}{2} (5x - 1) \right].$$

The top panel of Figure 11 shows the predicted global spatio-temporal solution, for which the resulting prediction error is measured at $1.24e - 02$ in the relative L^2 -norm. A more detailed assessment of the predicted solution is presented in the bottom panel of Figure 11, which displays a comparison between the exact and the predicted solutions at different temporal snapshots $t = 0, 50, 100$. Through domain decomposition in time, the physics-informed DeepONet can accurately predict the traveling wave across a long-time horizon. We further investigate the performance of a conventional DeepONet model, which can be trained by minimizing the loss function $\mathcal{L}_{\text{data}}$ solely. As shown in Figure 12, the results of the vanilla DeepONet are slightly worse than the physics-informed DeepONet. This conclusion is further confirmed by a relatively large prediction error of $6.84e - 02$. For a more thorough comparison, we train both a vanilla DeepONet and a physics-informed DeepONet for different number of training data points (i.e, different number of samples u), and report the mean of the relative L^2 error of $s(x, t)$ over all 100 examples in the test data-set in Figure 13. Compared to vanilla DeepONets, the proposed physics-informed DeepONets can not only achieve better predictive accuracy, but also utilize the observed data more efficiently, therefore providing enhanced effectiveness in small data regime.

5 Discussion

We have presented an effective methodology for performing long-time integration of evolution equations, for which many popular ML-based approaches such as physics-informed neural networks (PINNs) often struggle to yield accurate results. The proposed approach avoids the high computational cost associated with training multiple networks [18, 39, 41, 11], and introduces a new effective way to temporal domain decomposition in which a single network needs to be trained only within a short-time interval, albeit across a distribution of initial conditions. Leveraging the framework of physics-informed DeepONets [33], we put forth a simple two-step process. First, we demonstrate how deep neural networks can parametrize and learn solution operators that map initial conditions to associated ODE/PDE solutions in a short-time interval. The trained can be then iteratively evaluated to construct the global ODE/PDE in large temporal domains, at any arbitrary spatio-temporal resolution, and across a range of initial conditions. The effectiveness and robustness of the proposed algorithms has been demonstrated in a series of detailed numerical experiments involving long-time simulation of evolution laws that describe inherently different physical processes, including wave propagation, reaction-diffusion dynamics, and stiff chemical kinetics.

Long-time integration is often one of the main bottlenecks in simulating complex multi-scale and multi-physics processes in science and engineering, with applications ranging from understanding the effect of anthropogenic pollution in ocean and atmospheric chemical transport, to designing fuel-efficient combustion engines, to elucidating the biophysical mechanisms underpinning cardiovascular disease, and beyond. Developing high-fidelity simulation tools for such problems is technically and computationally challenging due to the long-time duration of interest, the stochastic nature of fragmentation and turbulent mixing phenomena, the temperature dependency of thermal neutralization mechanisms, and the stiff dynamics of bio-chemical reactions. The methods presented in this work are a first step towards demonstrating feasibility for ML-based techniques in reducing computational costs and enabling the rapid and accurate emulation of such non-equilibrium processes in science and engineering.

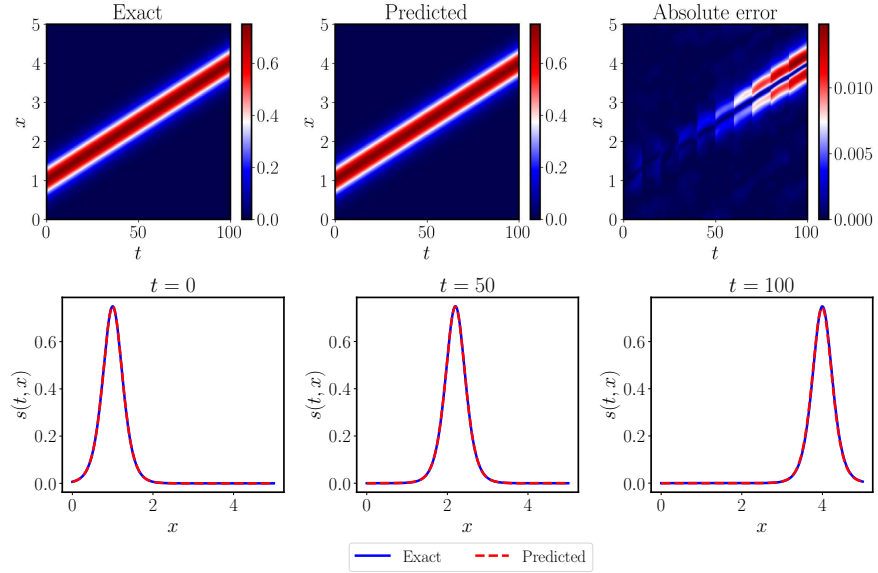


Figure 11: *Korteweg–De Vries equation*: *Top*: Exact solution versus the predicted solution of a trained physics-informed DeepONet using Algorithm 1 for integrating the PDE system (4.41) up to $T = 100$. The relative L^2 error is 1.24%. *Bottom*: Comparison between the exact and the predicted solutions at different temporal snapshots corresponding to $t = 0, 50, 100$.

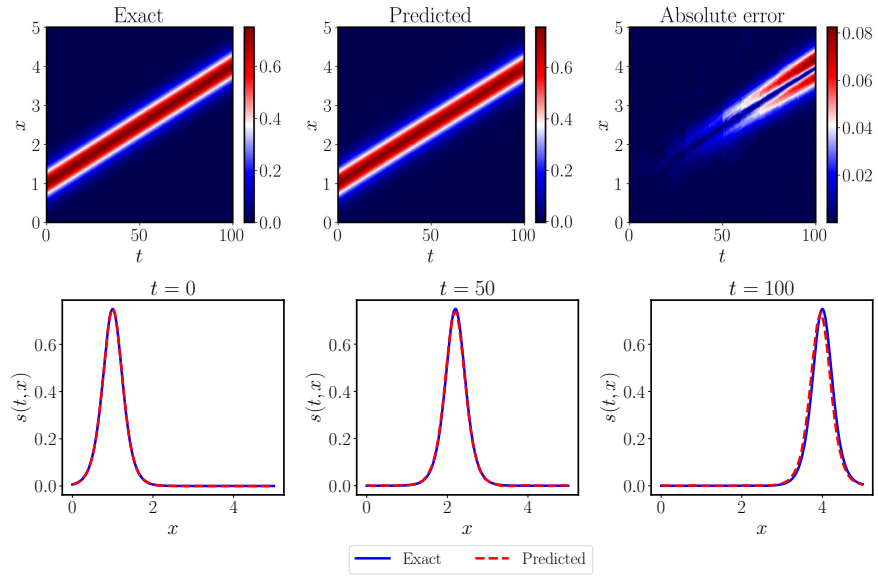


Figure 12: *Korteweg–De Vries equation*: *Top*: Exact solution versus the predicted solution of a trained conventional DeepONet using Algorithm 1 for integrating the PDE system (4.41) up to $T = 100$. The relative L^2 error is 6.84%. *Bottom*: Comparison between the exact and the predicted solutions at different temporal snapshots corresponding to $t = 0, 50, 100$.

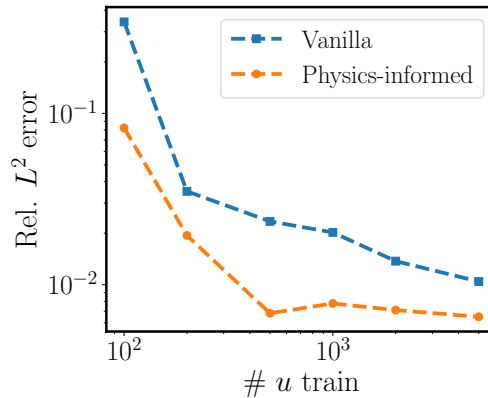


Figure 13: Relative L^2 prediction error of a vanilla DeepONet [42] versus the proposed physics-informed DeepONet as a function of the number of examples in the training data-set.

Despite the early promise demonstrated here, we have to admit that we are still at the very early stages of tackling long-time prediction problems with physics-informed DeepONets. There are many open questions worth considering as future research directions. From a theoretical point of view, it is important to develop a better understanding of how approximation errors affect the stability and accuracy of the proposed methods. This is a crucial element in applications that demand accuracy and convergence guarantees, where currently classical numerical solvers remain the de-facto choice. From a practical point of view, it would be intriguing to apply the proposed approach to solve chaotic dynamical systems, such as Kuramoto-Sivashinsky equation [53, 54] or the Navier-Stokes equations in the turbulent regime. These problems typically involve fast transitions of frequencies and are extremely sensitive to initial conditions, which inevitably introduces great challenges to both traditional numerical solvers, as well as ML-based approaches. From a methodology point of view, our algorithm can be regarded as a special "domain decomposition" in time, which further motivates us to develop domain decomposition in space with physics-informed DeepONets. This may be combined with traditional domain decomposition techniques such as the Schwartz alternating method [55] to open the path of scaling physics-informed ML approaches to large computational domains and complex geometries [56]. We believe that addressing these open questions will pave a new way to developing scientific machine learning algorithms with better robustness and accuracy guarantees, as needed for many critical applications in computational science and engineering.

Author Contributions

SW and PP conceptualized the research and designed the numerical studies. SW implemented the methods and conducted the numerical experiments. PP provided funding and supervised all aspects of this work. All authors contributed in writing the manuscript.

Acknowledgements

This work received support from DOE grant DE-SC0019116, AFOSR grant FA9550-20-1-0060, and DOE-ARPA grant DE-AR0001201. We would also like to thank the developers of the software that enabled our research, including JAX [50], Matplotlib [57], NumPy [58] and DeepXDE [59].

References

- [1] Richard Courant and David Hilbert. *Methods of Mathematical Physics: Partial Differential Equations*. John Wiley & Sons, 2008.
- [2] Parviz Moin. *Fundamentals of engineering numerical analysis*. Cambridge University Press, 2010.
- [3] Arieh Iserles. *A first course in the numerical analysis of differential equations*. Number 44. Cambridge university press, 2009.
- [4] Thomas JR Hughes. *The finite element method: linear static and dynamic finite element analysis*. Courier Corporation, 2012.

- [5] Yousef Saad. *Iterative methods for sparse linear systems*. SIAM, 2003.
- [6] George Em Karniadakis, Ioannis G Kevrekidis, Lu Lu, Paris Perdikaris, Sifan Wang, and Liu Yang. Physics-informed machine learning. *Nature Reviews Physics*, pages 1–19, 2021.
- [7] Dimitris C Psychogios and Lyle H Ungar. A hybrid neural network-first principles approach to process modeling. *AIChE Journal*, 38(10):1499–1511, 1992.
- [8] Isaac E Lagaris, Aristidis Likas, and Dimitrios I Fotiadis. Artificial neural networks for solving ordinary and partial differential equations. *IEEE transactions on neural networks*, 9(5):987–1000, 1998.
- [9] Maziar Raissi, Paris Perdikaris, and George Em Karniadakis. Inferring solutions of differential equations using noisy multi-fidelity data. *Journal of Computational Physics*, 335:736–746, 2017.
- [10] Yifan Chen, Bamdad Hosseini, Houman Owhadi, and Andrew M Stuart. Solving and learning nonlinear PDEs with gaussian processes. *arXiv preprint arXiv:2103.12959*, 2021.
- [11] Maziar Raissi, Hessam Babaei, and Peyman Givi. Deep learning of turbulent scalar mixing. *Physical Review Fluids*, 4(12):124501, 2019.
- [12] Sifan Wang, Yujun Teng, and Paris Perdikaris. Understanding and mitigating gradient pathologies in physics-informed neural networks. *arXiv preprint arXiv:2001.04536*, 2020.
- [13] Sifan Wang, Xinling Yu, and Paris Perdikaris. When and why PINNs fail to train: A neural tangent kernel perspective. *arXiv preprint arXiv:2007.14527*, 2020.
- [14] Sifan Wang, Hanwen Wang, and Paris Perdikaris. On the eigenvector bias of Fourier feature networks: From regression to solving multi-scale PDEs with physics-informed neural networks. *arXiv preprint arXiv:2012.10047*, 2020.
- [15] Maziar Raissi, Paris Perdikaris, and George E Karniadakis. Physics-informed neural networks: A deep learning framework for solving forward and inverse problems involving nonlinear partial differential equations. *Journal of Computational Physics*, 378:686–707, 2019.
- [16] Ehsan Kharazmi, Zhongqiang Zhang, and George Em Karniadakis. Variational physics-informed neural networks for solving partial differential equations. *arXiv preprint arXiv:1912.00873*, 2019.
- [17] Ameysa D Jagtap and George Em Karniadakis. Extended physics-informed neural networks (XPINNs): A generalized space-time domain decomposition based deep learning framework for nonlinear partial differential equations. *Communications in Computational Physics*, 28(5):2002–2041, 2020.
- [18] Xuhui Meng, Zhen Li, Dongkun Zhang, and George Em Karniadakis. PPINN: Parareal physics-informed neural network for time-dependent PDEs. *Computer Methods in Applied Mechanics and Engineering*, 370:113250, 2020.
- [19] Yin hao Zhu, Nicholas Zabaras, Phaedon-Stelios Koutsourelakis, and Paris Perdikaris. Physics-constrained deep learning for high-dimensional surrogate modeling and uncertainty quantification without labeled data. *Journal of Computational Physics*, 394:56–81, 2019.
- [20] Nicholas Geneva and Nicholas Zabaras. Modeling the dynamics of PDE systems with physics-constrained deep auto-regressive networks. *Journal of Computational Physics*, 403:109056, 2020.
- [21] Alvaro Sanchez-Gonzalez, Jonathan Godwin, Tobias Pfaff, Rex Ying, Jure Leskovec, and Peter Battaglia. Learning to simulate complex physics with graph networks. In *International Conference on Machine Learning*, pages 8459–8468. PMLR, 2020.
- [22] Maziar Raissi, Alireza Yazdani, and George Em Karniadakis. Hidden fluid mechanics: Learning velocity and pressure fields from flow visualizations. *Science*, 367(6481):1026–1030, 2020.
- [23] AM Tartakovsky, C Ortiz Marrero, Paris Perdikaris, GD Tartakovsky, and D Barajas-Solano. Physics-informed deep neural networks for learning parameters and constitutive relationships in subsurface flow problems. *Water Resources Research*, 56(5):e2019WR026731, 2020.
- [24] Oliver Hennigh, Susheela Narasimhan, Mohammad Amin Nabian, Akshay Subramaniam, Kaustubh Tangali, Max Rietmann, Jose del Aguila Ferrandis, Wonmin Byeon, Zhiwei Fang, and Sanjay Choudhry. Nvidia simnetTM: an ai-accelerated multi-physics simulation framework. *arXiv preprint arXiv:2012.07938*, 2020.
- [25] Shengze Cai, Zhicheng Wang, Sifan Wang, Paris Perdikaris, and George Em Karniadakis. Physics-informed neural networks for heat transfer problems. *Journal of Heat Transfer*, 143(6), 2021.
- [26] Georgios Kissas, Yibo Yang, Eileen Hwuang, Walter R Witschey, John A Detre, and Paris Perdikaris. Machine learning in cardiovascular flows modeling: Predicting arterial blood pressure from non-invasive 4D flow MRI data using physics-informed neural networks. *Computer Methods in Applied Mechanics and Engineering*, 358:112623, 2020.

- [27] Francisco Sahli Costabal, Yibo Yang, Paris Perdikaris, Daniel E Hurtado, and Ellen Kuhl. Physics-informed neural networks for cardiac activation mapping. *Frontiers in Physics*, 8:42, 2020.
- [28] Lu Lu, Ming Dao, Punit Kumar, Upadrasta Ramamurty, George Em Karniadakis, and Subra Suresh. Extraction of mechanical properties of materials through deep learning from instrumented indentation. *Proceedings of the National Academy of Sciences*, 117(13):7052–7062, 2020.
- [29] Yuyao Chen, Lu Lu, George Em Karniadakis, and Luca Dal Negro. Physics-informed neural networks for inverse problems in nano-optics and metamaterials. *Optics express*, 28(8):11618–11633, 2020.
- [30] Somdatta Goswami, Cosmin Anitescu, Souvik Chakraborty, and Timon Rabczuk. Transfer learning enhanced physics informed neural network for phase-field modeling of fracture. *Theoretical and Applied Fracture Mechanics*, 106:102447, 2020.
- [31] Dennis Elbrächter, Philipp Grohs, Arnulf Jentzen, and Christoph Schwab. Dnn expression rate analysis of high-dimensional PDEs: Application to option pricing. *arXiv preprint arXiv:1809.07669*, 2018.
- [32] Jiequn Han, Arnulf Jentzen, and E Weinan. Solving high-dimensional partial differential equations using deep learning. *Proceedings of the National Academy of Sciences*, 115(34):8505–8510, 2018.
- [33] Sifan Wang, Hanwen Wang, and Paris Perdikaris. Learning the solution operator of parametric partial differential equations with physics-informed DeepOnets. *arXiv preprint arXiv:2103.10974*, 2021.
- [34] Atilim Gunes Baydin, Barak A Pearlmutter, Alexey Andreyevich Radul, and Jeffrey Mark Siskind. Automatic differentiation in machine learning: a survey. *Journal of machine learning research*, 18, 2018.
- [35] Levi McClenny and Ulisses Braga-Neto. Self-adaptive physics-informed neural networks using a soft attention mechanism. *arXiv preprint arXiv:2009.04544*, 2020.
- [36] Diederik P Kingma and Jimmy Ba. Adam: A method for stochastic optimization. *arXiv preprint arXiv:1412.6980*, 2014.
- [37] Nasim Rahaman, Aristide Baratin, Devansh Arpit, Felix Draxler, Min Lin, Fred Hamprecht, Yoshua Bengio, and Aaron Courville. On the spectral bias of neural networks. In *International Conference on Machine Learning*, pages 5301–5310, 2019.
- [38] Matthew Tancik, Pratul P Srinivasan, Ben Mildenhall, Sara Fridovich-Keil, Nithin Raghavan, Utkarsh Singhal, Ravi Ramamoorthi, Jonathan T Barron, and Ren Ng. Fourier features let networks learn high frequency functions in low dimensional domains. *arXiv preprint arXiv:2006.10739*, 2020.
- [39] Colby L Wight and Jia Zhao. Solving Allen-Cahn and Cahn-Hilliard equations using the adaptive physics informed neural networks. *arXiv preprint arXiv:2007.04542*, 2020.
- [40] E Weinan. *Principles of multiscale modeling*. Cambridge University Press, 2011.
- [41] Yifan Du and Tamer A Zaki. Evolutional deep neural network. *arXiv preprint arXiv:2103.09959*, 2021.
- [42] Lu Lu, Pengzhan Jin, Guofei Pang, Zhongqiang Zhang, and George Em Karniadakis. Learning nonlinear operators via DeepONet based on the universal approximation theorem of operators. *Nature Machine Intelligence*, 3(3):218–229, 2021.
- [43] Andreas Griewank et al. On automatic differentiation. *Mathematical Programming: recent developments and applications*, 6(6):83–107, 1989.
- [44] Xavier Glorot and Yoshua Bengio. Understanding the difficulty of training deep feedforward neural networks. In *Proceedings of the thirteenth international conference on artificial intelligence and statistics*, pages 249–256, 2010.
- [45] Chelsea Finn, Pieter Abbeel, and Sergey Levine. Model-agnostic meta-learning for fast adaptation of deep networks. In *International Conference on Machine Learning*, pages 1126–1135. PMLR, 2017.
- [46] Weiqi Ji, Weilun Qiu, Zhiyu Shi, Shaowu Pan, and Sili Deng. Stiff-PINN: Physics-informed neural network for stiff chemical kinetics. *arXiv preprint arXiv:2011.04520*, 2020.
- [47] Gerhard Wanner and Ernst Hairer. *Solving ordinary differential equations II*, volume 375. Springer Berlin Heidelberg, 1996.
- [48] HH Robertson. The solution of a set of reaction rate equations. *Numerical analysis: an introduction*, 178182, 1966.
- [49] Ernst Hairer and Gerhard Wanner. Stiff differential equations solved by radau methods. *Journal of Computational and Applied Mathematics*, 111(1-2):93–111, 1999.

- [50] James Bradbury, Roy Frostig, Peter Hawkins, Matthew James Johnson, Chris Leary, Dougal Maclaurin, George Necula, Adam Paszke, Jake VanderPlas, Skye Wanderman-Milne, and Qiao Zhang. JAX: composable transformations of Python+NumPy programs, 2018.
- [51] Klaus Brauer. The Korteweg-de Vries equation: history, exact solutions, and graphical representation. *University of Osnabrück/Germany1*, 2000.
- [52] John W Miles. The Korteweg-de Vries equation: a historical essay. *Journal of fluid mechanics*, 106:131–147, 1981.
- [53] GI Sivashinsky. Nonlinear analysis of hydrodynamic instability in laminar flames—i. derivation of basic equations. *AcAau*, 4(11):1177–1206, 1977.
- [54] Yoshiki Kuramoto. Diffusion-induced chaos in reaction systems. *Progress of Theoretical Physics Supplement*, 64:346–367, 1978.
- [55] Pierre-Louis Lions. On the Schwarz alternating method. i. In *First international symposium on domain decomposition methods for partial differential equations*, volume 1, page 42. Paris, France, 1988.
- [56] Hengjie Wang, Robert Planas, Aparna Chandramowlishwaran, and Ramin Bostanabad. Train once and use forever: Solving boundary value problems in unseen domains with pre-trained deep learning models. *arXiv preprint arXiv:2104.10873*, 2021.
- [57] John D Hunter. Matplotlib: A 2D graphics environment. *IEEE Annals of the History of Computing*, 9(03):90–95, 2007.
- [58] Charles R Harris, K Jarrod Millman, Stéfan J van der Walt, Ralf Gommers, Pauli Virtanen, David Cournapeau, Eric Wieser, Julian Taylor, Sebastian Berg, Nathaniel J Smith, et al. Array programming with numpy. *Nature*, 585(7825):357–362, 2020.
- [59] Lu Lu, Xuhui Meng, Zhiping Mao, and George Em Karniadakis. DeepXDE: A deep learning library for solving differential equations. *SIAM Review*, 63(1):208–228, 2021.

A Notations

Table 1 summarizes the main symbols and notation used in this work.

Notation	Description
$u(\cdot)$	an input function
$s(\cdot)$	a solution to a parametric PDE
G	an operator
G_{θ}	an DeepONet representation of the operator G
θ	all trainable parameters of a DeepONet
$\{\mathbf{x}_i\}_{i=1}^m$	m sensor points where input functions $u(\mathbf{x})$ are evaluated
$[u(\mathbf{x}_1), u(\mathbf{x}_2), \dots, u(\mathbf{x}_m)]$	an input of the branch net, representing the input function u
N	# input samples in the training data-set
m	# locations for evaluating the input functions u
P	# locations for evaluating the output functions $G(u)$
Q	# collocation points for evaluating the PDE residual
GRF	a Gaussian random field
l	length scale of a Gaussian random field

Table 1: *Nomenclature*: Summary of the main symbols and notation used in this work.

B Hyper-parameter settings

Table 2 summarizes the hyper-parameter setting for all examples considered in this work.

Case	Input function space	m	P	Q	#u Train	# u Test	Iterations
Gravity pendulum	$\mathcal{U}(-3, 3)$	1	1	100	5×10^4	100	3×10^5
Linear ODE	GRF ($l = 0.5$) & $\mathcal{U}(-2, 2)$	100 & 1	1	100	5×10^4	100	2×10^5
Stiff ODE	$\mathcal{U}(0, 1)$	1	1	10^3	5×10^4	100	4×10^5
Wave equation	GRF($l = 0.5$)	100	100	200	10^4	100	2×10^5
Diffusion-reaction equation	GRF($l=0.2$)	100	100	100	10^4	100	2×10^5
KDV equation	$\mathcal{U}(1, 2) \times \mathcal{U}(0, 5)$	200	200	200	5×10^3	100	2×10^5

Table 2: Default hyper-parameter settings for each benchmark employed in this work (unless otherwise stated).

Case	Trunk depth	Trunk width	Branch depth	Branch width
Gravity pendulum	8	100	8	100
Linear ODE	7	100	7	100
Stiff ODE	7	100	7	100
Wave equation	5	200	5	200
Diffusion-reaction equation	5	100	5	100
KDV equation	7	200	7	200

Table 3: DeepONet architectures for each benchmark employed in this work (unless otherwise stated).

C Performance metrics

The error metric employed throughout all numerical experiments to assess model performance is the relative L^2 norm. Specifically, the reported test errors correspond to the mean of the relative L^2 error of a trained physics-informed DeepONet model over all examples in the test data-set, i.e

$$\text{Test error} := \frac{1}{N} \sum_{i=1}^N \frac{\|G_\theta(\mathbf{u}^{(i)})(y) - G(\mathbf{u}^{(i)})(y)\|_2}{\|G(\mathbf{u}^{(i)})(y)\|_2}, \quad (\text{C.1})$$

where N denotes the number of examples in the test data-set and y is typically a set of equi-spaced points in the domain of $G(u)$. Here $G_\theta(\mathbf{u}^{(i)})(y)$ denotes the predicted DeepONet outputs, while $G(\mathbf{u}^{(i)})(y)$ corresponds to the ground truth target functions.

D Computational cost

Training: Table 4 summarizes the computational cost (hours) of training different models. The size of different models as well as network architectures are listed Table 3. All networks are trained using a single A100 card. It can be observed that training a physics-informed DeepONet model is generally slower than training a conventional DeepONet. This is expected as physics-informed DeepONets require to compute the PDE residual via automatic differentiation, yielding a larger computational graph, and, therefore, a higher computational cost.

Case	Model	Training time (hours)
Gravity pendulum	Physics-informed neural network	0.12
	Physics-informed DeepONet	1.63
Linear ODE	Physics-informed DeepONet	1.33
Stiff ODE	Physics-informed DeepONet	7.60
Wave equation	Physics-informed DeepONet	3.00
Diffusion-reaction equation	Physics-informed DeepONet	1.48
KDV equation	Physics-informed DeepONet	2.17
	DeepONet	0.35

Table 4: Computational cost (hours) for training different models across the different benchmarks and architectures employed in this work. Reported timings are obtained on a single Nvidia V100 GPU.

Inference: Once trained, the model can be rapidly queried to return prediction at short-time intervals. Each query typically takes $\mathcal{O}(10^{-3})$ ms on a single Nvidia V100 GPU. Constructing the global PDE/ODE solution in large temporal domains using Algorithm 1 requires $N \sim \mathcal{O}(10) - \mathcal{O}(10^3)$ evaluations of the trained model, typically leading to a total inference time of $\sim \mathcal{O}(10^{-2})$ sec for a given initial condition. Multiple initial conditions can also be simulated at once, as our JAX [50] implementation is trivially vectorized and parallelized on GPU hardware. As demonstrated in Figure 7, the proposed framework can perform long-time integration of more than 1,000 initial conditions in $\mathcal{O}(1)$ second, yielding a $\sim 10x-50x$ speedup compared to a traditional numerical solver. Unlike traditional numerical solvers that are heavily specialized to a specific type of dynamic behavior, this cost remains nearly constant for all examples considered in this work, regardless of the ODE/PDE system that is simulated, as it merely amounts to the cost associated with evaluating the forward pass of the trained DeepONet model.

E Supplementary Figures

E.1 Gravity pendulum

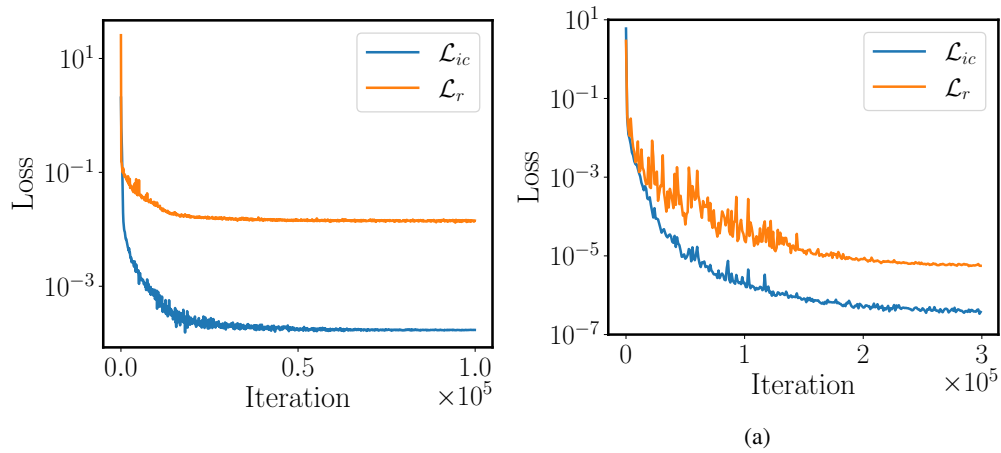


Figure 14: *Gravity pendulum*: *Left*: Training loss convergence of a conventional PINN model for 10^5 iterations of gradient descent using the Adam optimizer. *Right*: Training loss convergence of a physics-informed DeepONet model for 3×10^5 iterations of gradient descent using the Adam optimizer.

E.2 Inhomogeneous ODE

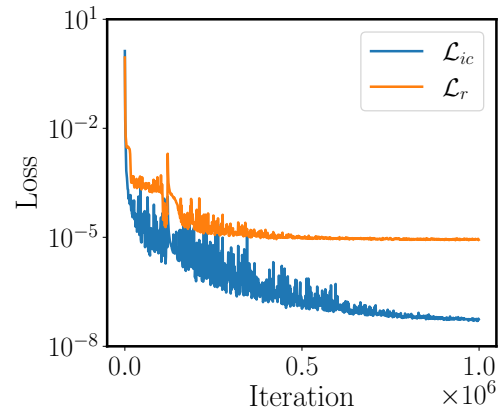


Figure 15: *Linear ODE*: Training loss convergence of a physics-informed DeepONet model for 10^5 iterations of gradient descent using the Adam optimizer.

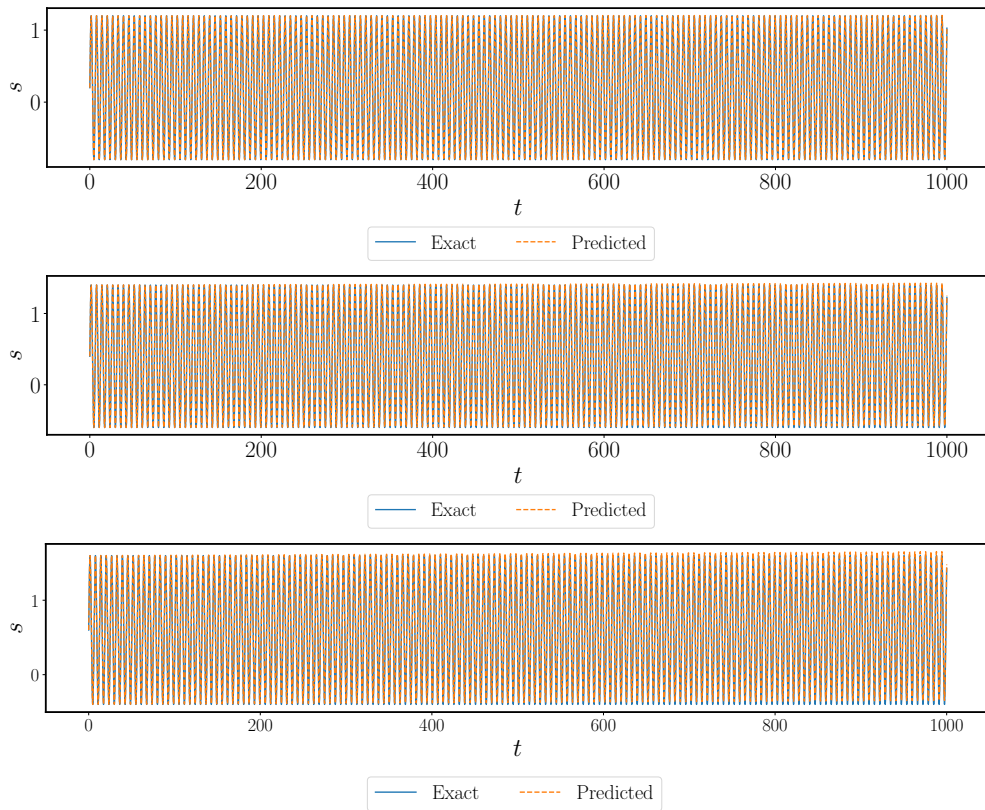


Figure 16: *Linear ODE*: Predicted solutions obtained by a trained physics-informed DeepONet using Algorithm 1, across three different initial conditions $s(0) = 0.2, 0.4, 0.6$. The relative L^2 errors are 0.52%, 1.79%, 3.30% respectively.

E.3 Stiff chemical kinetics

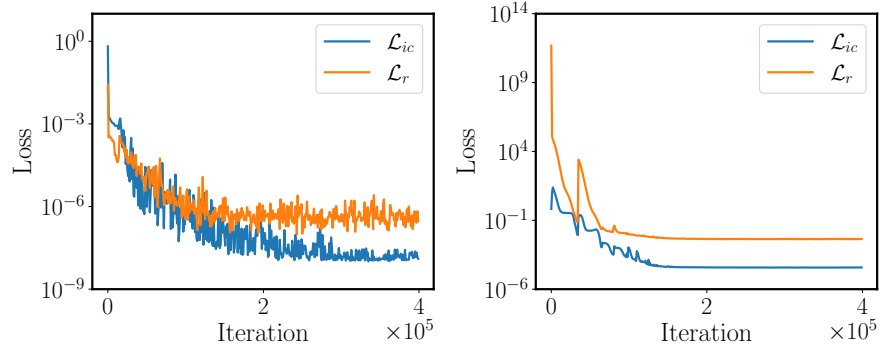


Figure 17: *Stiff ODE*: *Left*: Training loss convergence of a scaled physics-informed DeepONet model for 4×10^5 iterations of gradient descent using the Adam optimizer. *Right*: Training loss convergence of an unscaled physics-informed DeepONet model for 4×10^5 iterations of gradient descent using the Adam optimizer.

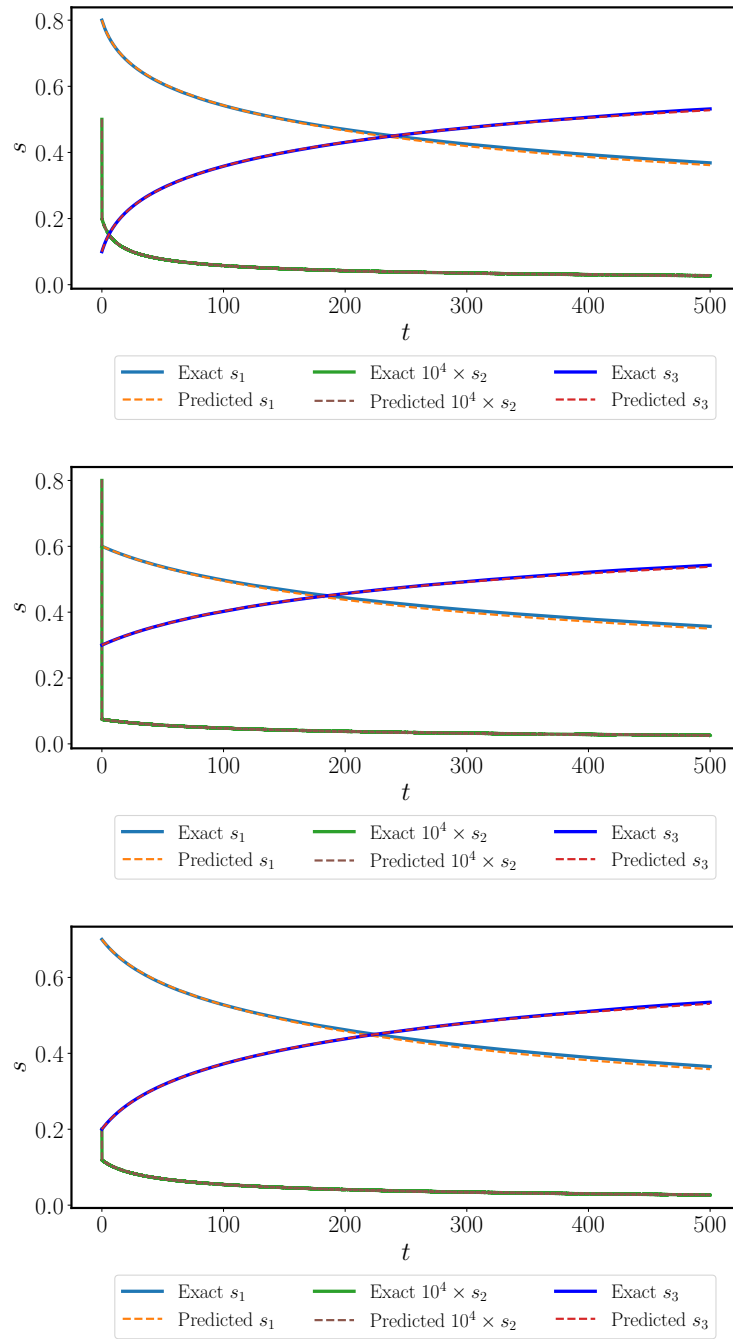


Figure 18: *Stiff ODE*: Predicted solutions of a trained physics-informed DeepONet using Algorithm 1 for three different initial conditions.

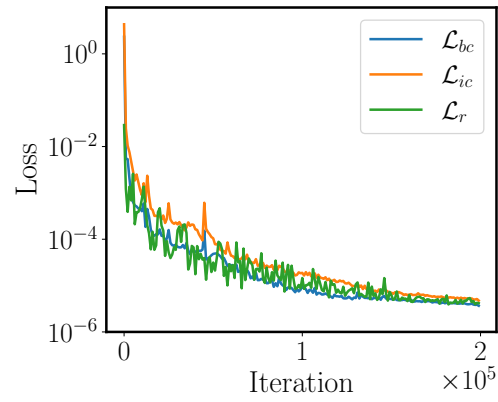
E.4 Wave propagation

Figure 19: *Wave equation*: Training loss convergence of a physics-informed DeepONet model for 2×10^5 iterations of gradient descent using the Adam optimizer.

E.5 Diffusion-reaction dynamics

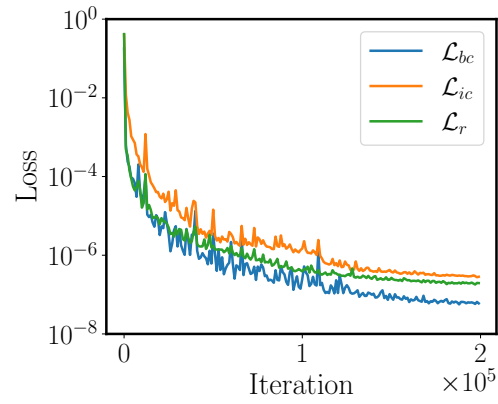


Figure 20: *Diffusion-reaction system*: Training loss convergence of a physics-informed DeepONet model for 2×10^5 iterations of gradient descent using the Adam optimizer.

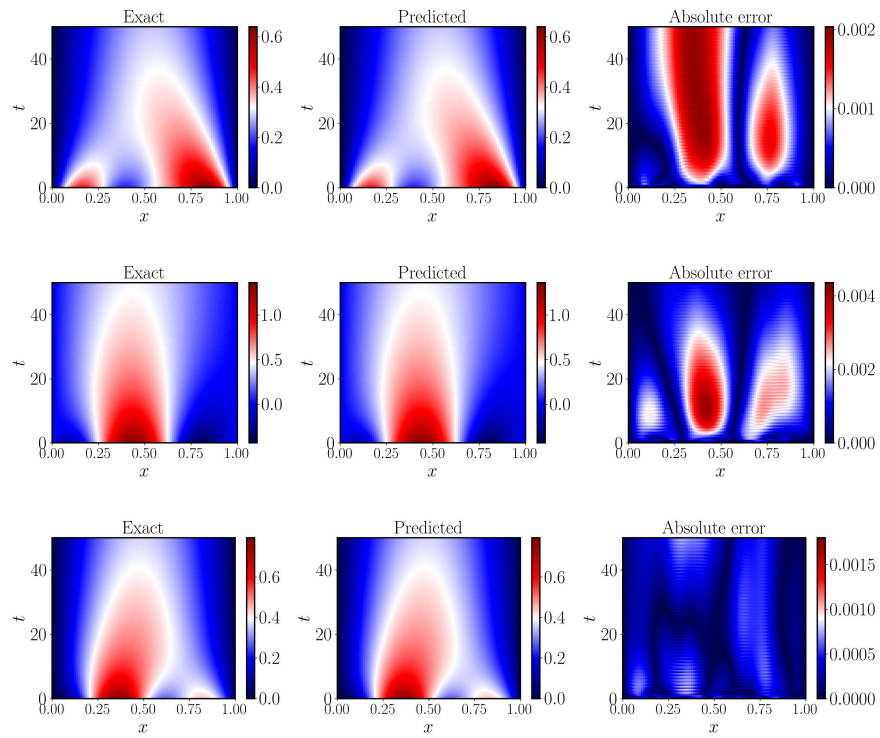


Figure 21: *Diffusion-reaction system*: Predicted solutions of a trained physics-informed DeepONet using Algorithm 1 for three different initial conditions.

E.6 KDV equation

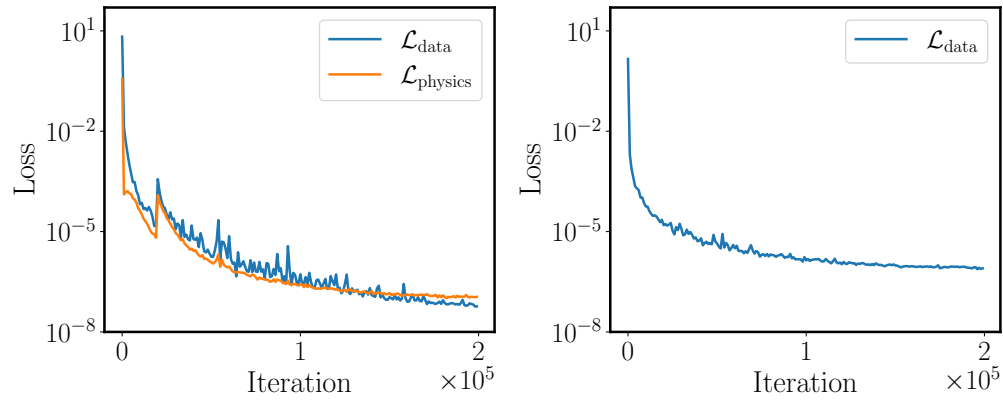


Figure 22: *Stiff ODE*: *Left*: Training loss convergence of a physics-informed DeepONet model for 2×10^5 iterations of gradient descent using the Adam optimizer. *Right*: Training loss convergence of a conventional DeepONet model for 2×10^5 iterations of gradient descent using the Adam optimizer.